NASA Technical Memorandum 100729

Analysis of Altimetry Over Inland Seas

A. Y. Au, R. D. Brown
and J. E. Welker

April 1989

(NASA-TM-100729) ANALYSIS OF ALTIMETRY OVER INLAND SEAS (NASA) 29 p
CSCL 08C

Unclas
G3/46 0272296

NASA

NASA Technical Memorandum 100729

Analysis of Altimetry Over Inland Seas

A. Y. Au and R. D. Brown
ST Systems Corporation (STX)
Lanham, Maryland

J. E. Welker
Geodynamics Branch
Laboratory for Terrestrial Physics
Goddard Space Flight Center
Greenbelt, Maryland

National Aeronautics and
Space Administration

Goddard Space Flight Center
Greenbelt, Maryland

1989

PREFACE

Satellite-based altimetric data taken by GEOS-3 and SEASAT over the Black Sea and Caspian Sea are analyzed and a least-squares collocation technique is used to predict the geoid undulations on a .25° x .25° grid and to transform these geoid undulations to free air gravity anomalies. Rapp's 180 x 180 geopotential model is used as the reference surface for the collocation procedure. The result of geoid to gravity transformation is, however, sensitive to geographic variability in the information content of the reference geopotential model used. For example, detailed surface gravity data are available for incorporation into the reference model over the Black Sea, resulting in a reference model with significant information content at short wavelengths. It is shown that reliable estimation of gravity anomalies from gridded geoid heights is generally possible over regions such as the Black Sea, using the conventional collocation technique. Over regions where surface data are generally not available for incorporation into the reference model, such as the Caspian Sea, an enhanced algorithm is needed to obtain reliable gravity anomalies. A feasible algorithm would extract both short and long wavelength information from the altimetric geoid heights and create an accurate gravity field at all wavelengths. Methods of generating such an algorithm are described and tested.

PRECEDING PAGE BLANK NOT FILMED

PAGE iii INTENTIONALLY BLANK

TABLE OF CONTENTS

List of Figures

List of Tables

Acknowledgements

The authors would like to express their gratitude to Dr. Huseyin Iz for his critical review of the manuscript. Richard Ullman is also to be thanked for his helpful comments on the manuscript.

I. INTRODUCTION

This project entailed processing satellite altimeter data over inland seas (the Black and Caspian Seas) for recovery of area mean gravity information. Gravity information in this area of the world is not readily available, so the possibility of obtaining it from the processing of altimeter observations is attractive. The mean surface level of the seas approximates an equipotential surface. Therefore, information about the underlying gravity potential and its derivative, gravity, can be obtained from measurement of the relative shape of this surface by means of altimetry.

Our principal objective on this project was to complete and extend analyses done in a previous study, verify those results, and document the results and techniques. A secondary objective was to improve the algorithms and results, if possible. The basic approach used by the previous study, and followed by STX personnel, involved five steps:

1. Edit geoid height data to remove overland data;
2. Evaluate geoid height differences at crossover points;
3. Remove orbit errors from geoid heights using crossover differences;
4. Grid geoid height data at 0.25° x 0.25° intervals;
5. Estimate 0.25° x 0.25° gravity anomalies from gridded geoid heights using the collocation technique.

The need for step 1 is obvious. Steps 2 and 3 are necessary because satellite altimeter measurements cannot yield accurate sea surface heights unless differences in satellite heights (orbit differences) from pass to pass are rectified and reduced to a common reference. If the mean sea surface height at a given location is constant over the time span of the altimeter data used, any difference in surface height between two altimeter passes at the point where they cross is due to orbit differences (differences of up to about 50 cm could be a consequence

of tides, especially solid earth tides, whose amplitudes are about 25 cm). Since the orbit differences are constant for the short arcs over the inland seas, removal of a constant bias from all the crossover differences of a given pass should effectively rectify orbit differences. Area mean surface height values are determined and reduced to the reference geoid in step 4. In step 5 these area mean geoid heights are processed and area mean gravity anomaly values are predicted using a linear least-squares estimation technique, called collocation, formulated by Moritz (1978). The collocation technique is essentially a differential operation transforming geopotential information to its first derivative, gravity. Knowledge of the statistical correlation between area mean geoid heights and gravity anomalies is required in the geoid-to-gravity transformation.

GEOS-3 altimeter data is of lesser quality (standard deviation between 25 and 50 cm, depending on operating mode) than that of SEASAT (6 to 10 cm), primarily because SEASAT uses an advanced radar altimeter design. The GEOS-3 altimeter operating modes, intensive and global, are differentiated primarily by data rate, which explains the corresponding difference in quality. The GEOS-3 mission collected data between 1975 and 1978 over latitudes up to 65 degrees, whereas SEASAT collected data only during 100 days in 1978 over latitudes up to 72 degrees.

In the next section, steps 1 to 4 are discussed in greater detail. An expanded mathematical description of the collocation technique and results of its application to both geoid gridding and gravity prediction are presented in Section III. The results of this project are discussed in Section IV. Conclusions and recommendations are presented in Section V.

II. ALTIMETER DATA

The altimeter data over the Black and Caspian Seas, obtained from NASA / GSFC, had been processed with GEODYN and written in GEODYN format. Program PRTDATA (Au *et al.*, 1989) organized the data records and extracted relevant geodetic and auxiliary information. There are 83 GEOS-3 and 62 SEASAT passes over the Black Sea written in 9,248 data records. Over the Caspian Sea there are 71 GEOS-3 and 23 SEASAT passes written in 20,642 data records. Program PLTGRP (Au *et al.*, 1989) was developed to plot the altimetric surface elevation of each pass as a function of time. Typical elevation profiles over the Black and Caspian Seas are shown in Figures 1 and 2, respectively. Visual examination of these surface elevation profiles suggests that the data are relatively noiseless, except for a few occurrences of data spikes and data gaps. In subsequent data processing programs, data spikes were eliminated by removing data points that deviated from adjacent ones by more than a given value, which was 2 meters for the Black Sea and 5 meters for the Caspian Sea. The ground tracks of these satellite passes over the Black and Caspian Seas, plotted with Program GRNTRK (Au *et al.*, 1989), are shown in Figures 3 and 4, respectively.

Crossover Adjustments

The major error source in altimetric geoid undulations is the uncertainty in the radial component of the satellite trajectory. This uncertainty is manifested in the misclosure of surface elevation at ground track intersections (crossovers) between passes. For the short arcs considered here, the orbit error can be modeled as a bias applied to all the data of a given pass. The optimum biases are such that crossover differences are minimized, holding one pass fixed so that all the satellite passes can be defined with respect to a common reference model.

ORIGINAL PAGE IS
OF POOR QUALITY

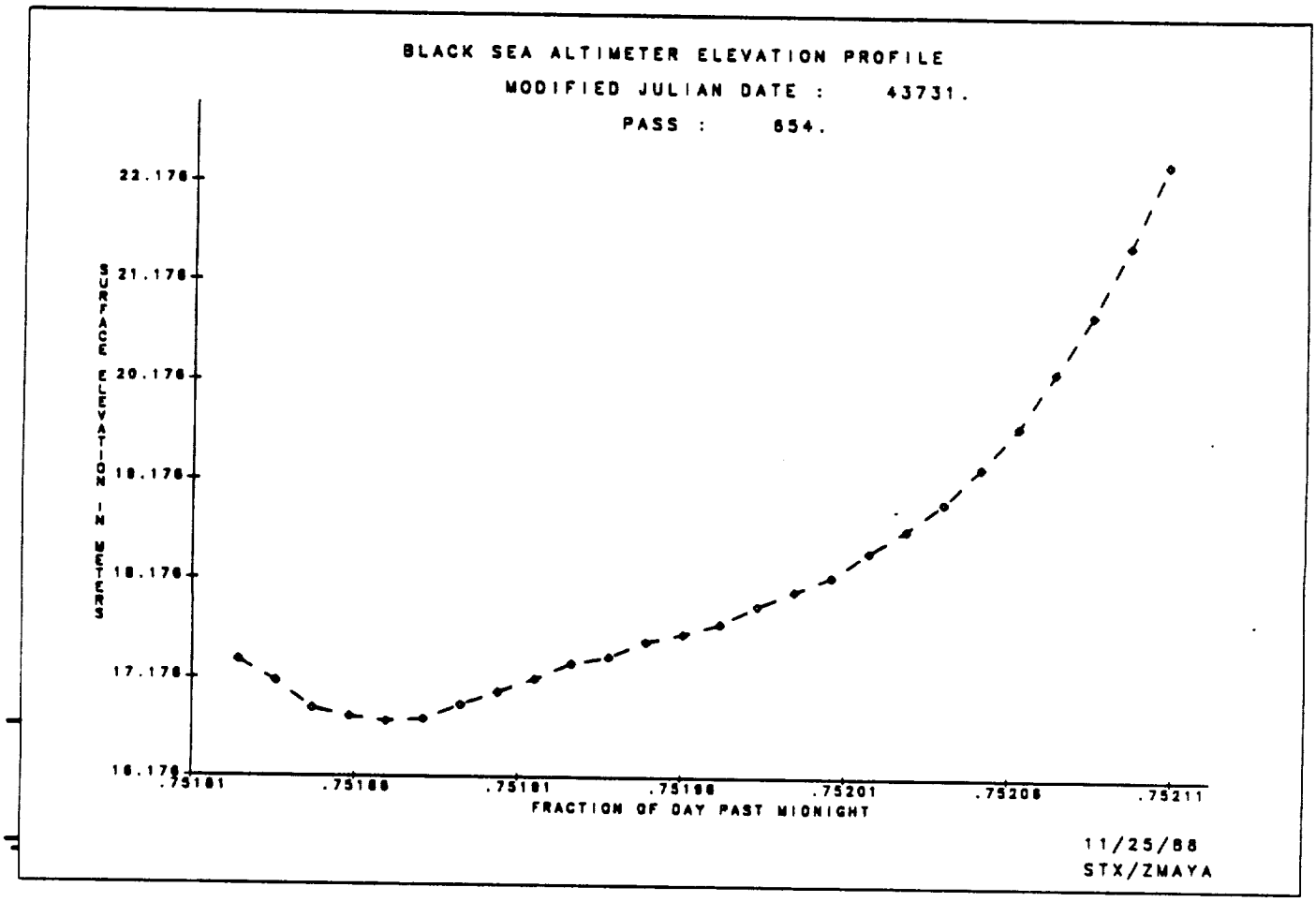

Figure 1a. Sample altimeter elevation profiles of the Black Sea.
Relatively noiseless profile.

ORIGINAL PAGE IS
OF POOR QUALITY

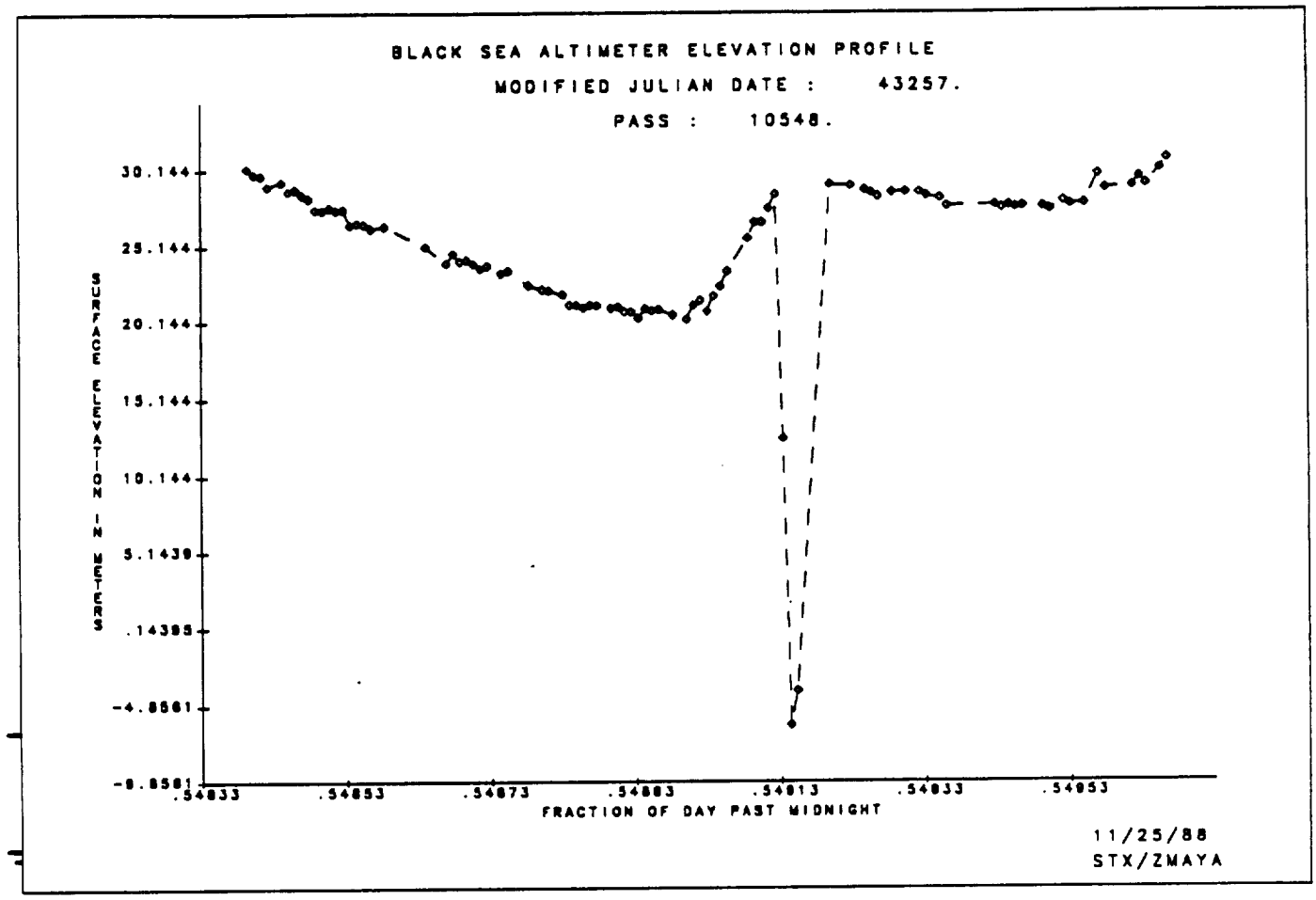

Figure 1b. Sample altimeter elevation profiles of the Black Sea.
Profile with data spike.

ORIGINAL PAGE IS
OF POOR QUALITY

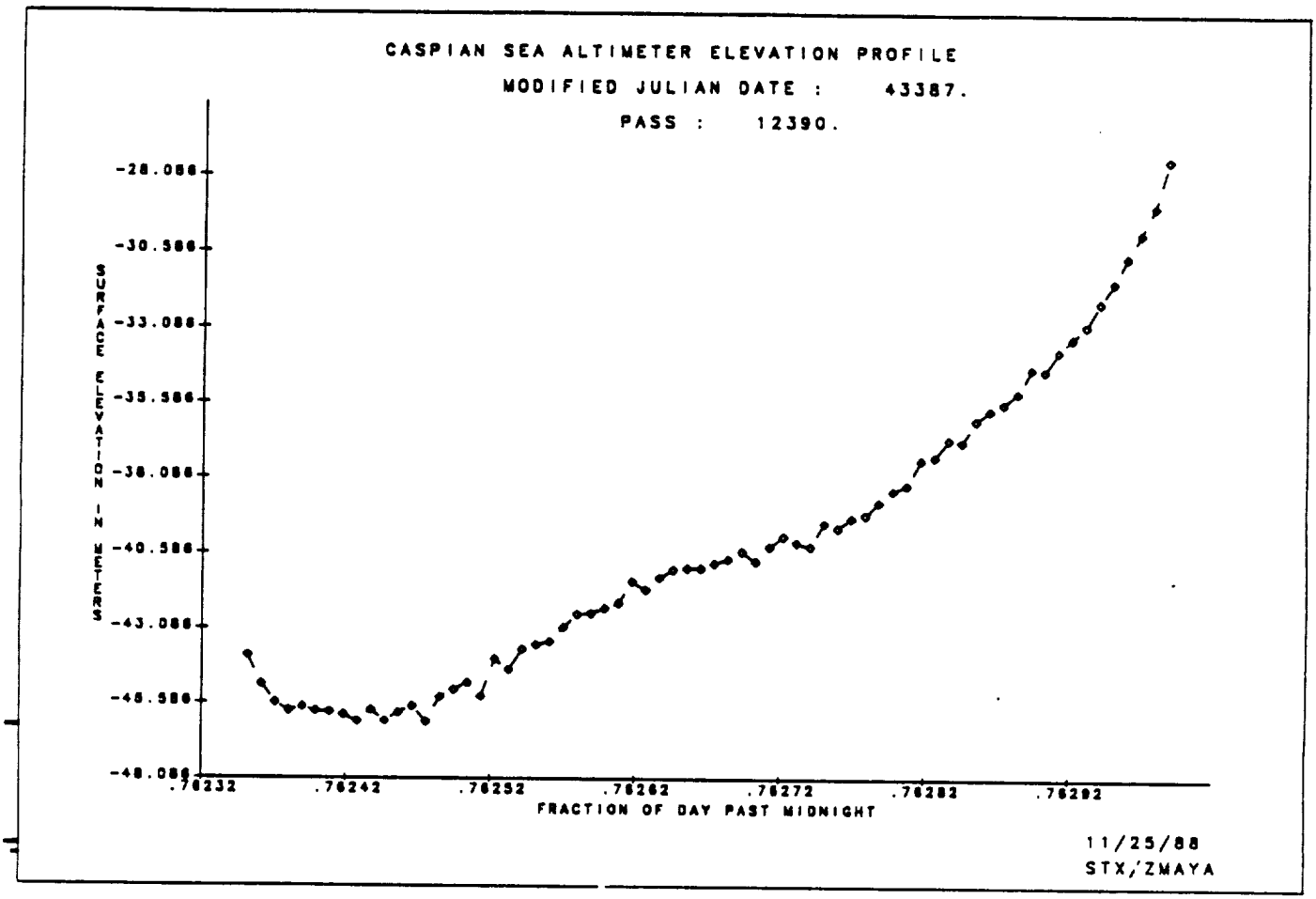

Figure 2a. Sample altimeter elevation profiles of the Caspian Sea.
Relatively noiseless profile.

ORIGINAL PAGE IS
OF POOR QUALITY

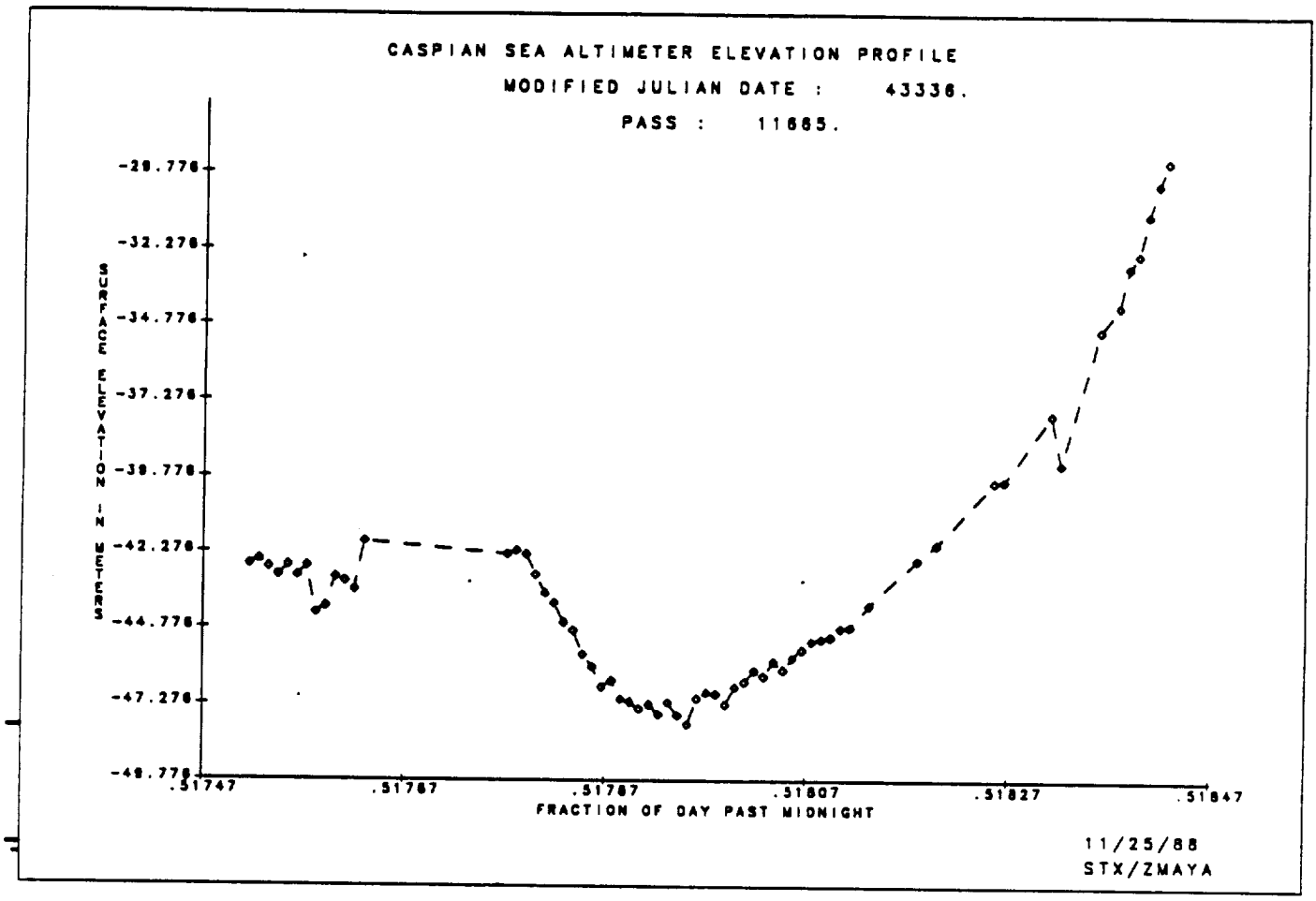

Figure 2b. Sample altimeter elevation profiles of the Caspian Sea.
Profile with data gap.

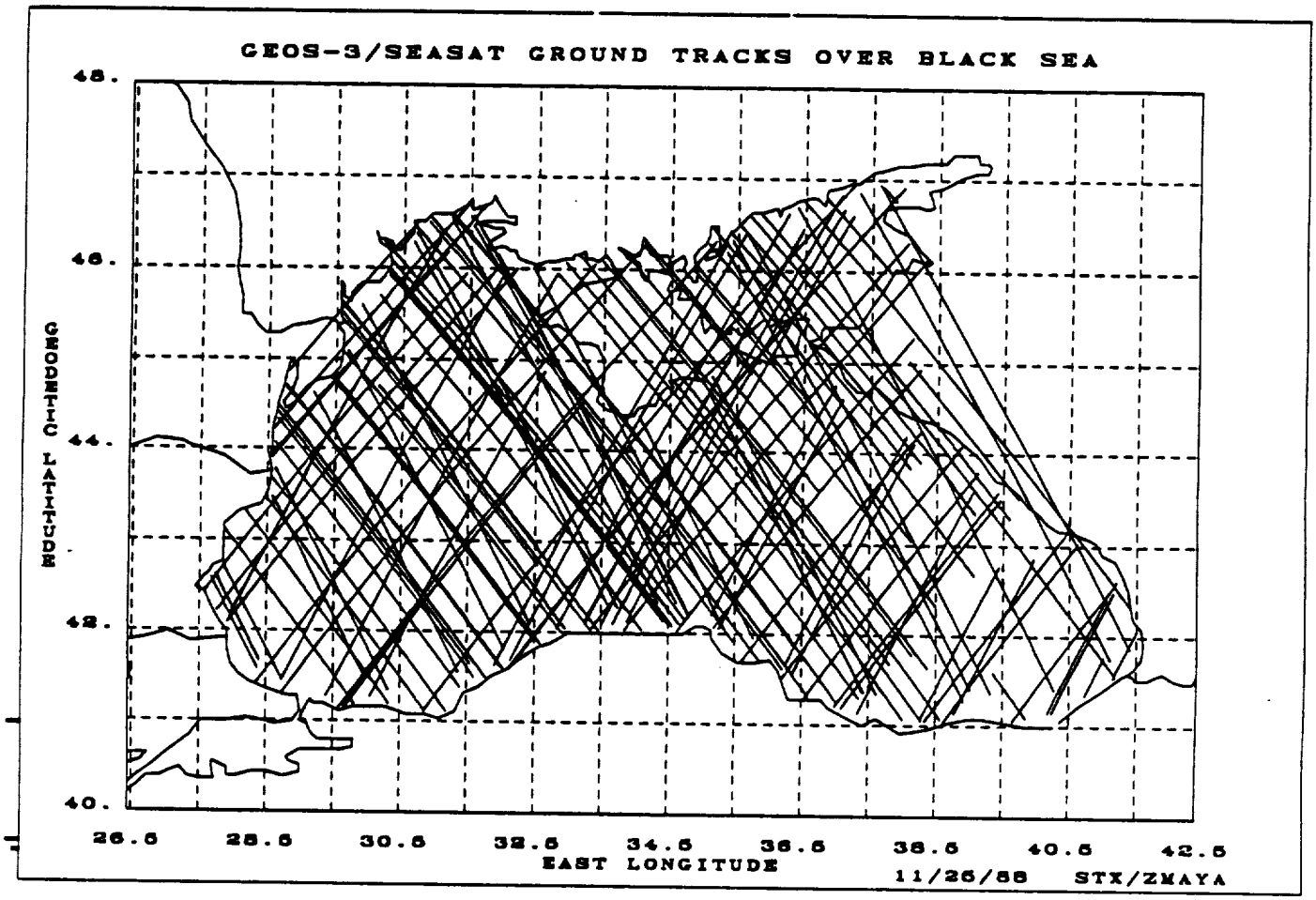

Figure 3. GEOS-3/SEASAT ground tracks over the Black Sea.

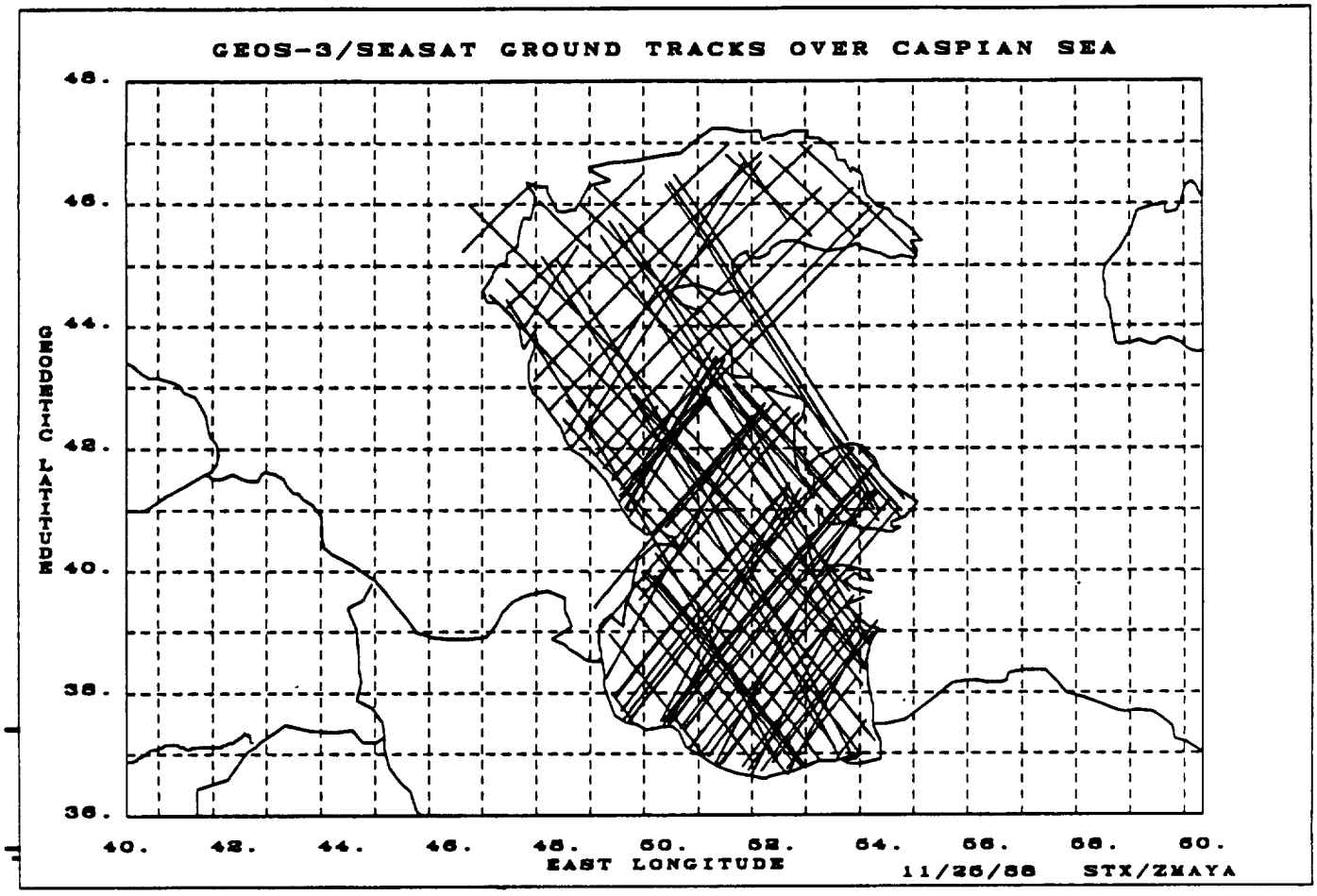

Figure 4. GEOS-3/SEASAT ground tracks over the Caspian Sea.

To calculate crossover differences, one must first locate the crossover location in latitude and longitude. There are various methods by which this point can be determined. We have adopted an analytical method of modeling the ground track of the pass. For relatively short arcs, such as the satellite passes over the Black and Caspian Seas, the ground track can be approximated by a second-degree equation,

$$Y = aX^2 + bX + c \tag{1}$$

where Y and X are, respectively, the latitude and longitude vectors of ground track records, and a, b and c are polynomial coefficients to be determined by fitting the ground track data using the method of least-squares. The error in this satellite arc representation is less than the radius of the illuminated area of the altimeter signal at the sea surface. The latitudes of the crossover point of two passes, Y_1 and Y_2, are set equal, $Y_1 = Y_2$. The longitude at which this crossover occurs is determined by solving the quadratic equation for X. An acceptable crossover point, naturally, must lie within the ground track records of both passes considered. Program XOVER0 (Au *et al.*, 1989) was used to determine the latitudes and longitudes of all possible crossovers and to prepare for subsequent crossover adjustments.

Once the crossover point is located, the altimetric height is interpolated by cubic splines from the nearest data for each pass. The true geoid undulation at a crossover point must be the same for both passes regardless of satellite and time. Altimetric height, however, is not exactly the same as geoid undulation. For example, temporal processes such as solid earth and ocean tides may cause the sea surface height to be different at the different times of the crossing altimeter passes. Ocean tides on small seas like these should contribute less than 10 cm to the crossover difference, but diurnal earth tides may be expected to contribute up to about 80 cm. Fortunately, tides are such broad-scale features in both space and time that they are manifest as a constant bias in a single pass of altimeter measurements over features as

small as the Black and Caspian Seas. Thus any earth tide effects alias with the orbit error bias and are removed when this bias is adjusted. To illustrate this adjustment, let H_t^O be the true geoid undulation for pass t at a crossover point and b_t be the bias assumed for this pass. The observed geoid undulation H_t is given by

$$H_t = H_t^O + b_t \quad . \tag{2}$$

The difference d_{tj} at a crossover point between pass t and pass J will be

$$\begin{aligned} d_{tj} &= H_t - H_J \\ &= (H_t^O + b_t) - (H_J^O + b_J) \\ &= b_t - b_J \end{aligned} \tag{3}$$

because H_t^O and H_J^O must be identical at a crossover point. An overdetermined system of equations in b results if all crossover residuals over an inland sea are considered. The bias for each pass, therefore, can be determined using the method of weighted least-squares, thus minimizing the crossover differences d. The standard error is assumed to be 25 cm for GEOS-3 and 10 cm for SEASAT in the weight matrix. The optimal pass bias vector B is given by

$$B = (\tilde{A}WA)^{-1}(\tilde{A}WD) \tag{4}$$

where D is the vector of crossover differences, W is a diagonal matrix in which diagonal elements are the sum of the inverse of the squares of the assumed sigma for each satellite. The matrix A is sparse. Each row of A contains all zeros except unitary value in the column associated with a pass t and a negative unitary value in the column associated with pass J.

The pass with the most crossovers was chosen as the reference pass. The bias for this pass is not estimated, but, after the crossover adjustment process, is assigned the average geoid height along the reference pass ground track, as calculated from the reference geopotential model. Rapp's 180 x 180 model is the reference geopotential model used in the current report. Program XOVER (Au *et al.*, 1989) was developed to perform the crossover adjustment process. An error covariance matrix of the crossover adjustment was also determined by XOVER. This error covariance matrix adds to the error associated with each satellite pass a crossover adjustment error.

From the geometry of altimeter passes in the current dataset, there are at most, 2109 crossovers over the Black Sea, 570 of which are GEOS-3 with GEOS-3, 383 are SEASAT with SEASAT and 1156 are GEOS-3 with SEASAT. These possible crossover locations were carefully checked in order to eliminate any crossover locations from further consideration if they occurred at data gaps, which are defined to be part of a satellite arc that did not have an altimeter observation within 70 km (about 10 seconds in time). Such editing reduced the number of crossovers to 1891, 521 of which are GEOS-3 with GEOS-3, 350 are SEASAT with SEASAT and 1020 are GEOS-3 with SEASAT. The RMS (root-mean-square) of the crossover residuals before crossover adjustment is 3.96 m. The RMS after crossover adjustment is reduced to 25 cm. The reference pass is the GEOS-3 pass #10557. Typical adjusted profiles and their corresponding reference models are shown in Figure 5. Program PLTAEP (Au *et al.*, 1989) was developed to plot the adjusted profiles.

We have analyzed these crossover difference statistics for consistency with the reported precision of the GEOS-3 and SEASAT altimeter data. Stanley (1979) reported the standard deviation of the GEOS-3 altimeter precision at 25 cm in the intensive mode, and 50 cm in the global mode. We have no knowledge of the mode of the GEOS-3 altimeter data used in this

ORIGINAL PAGE IS
OF POOR QUALITY

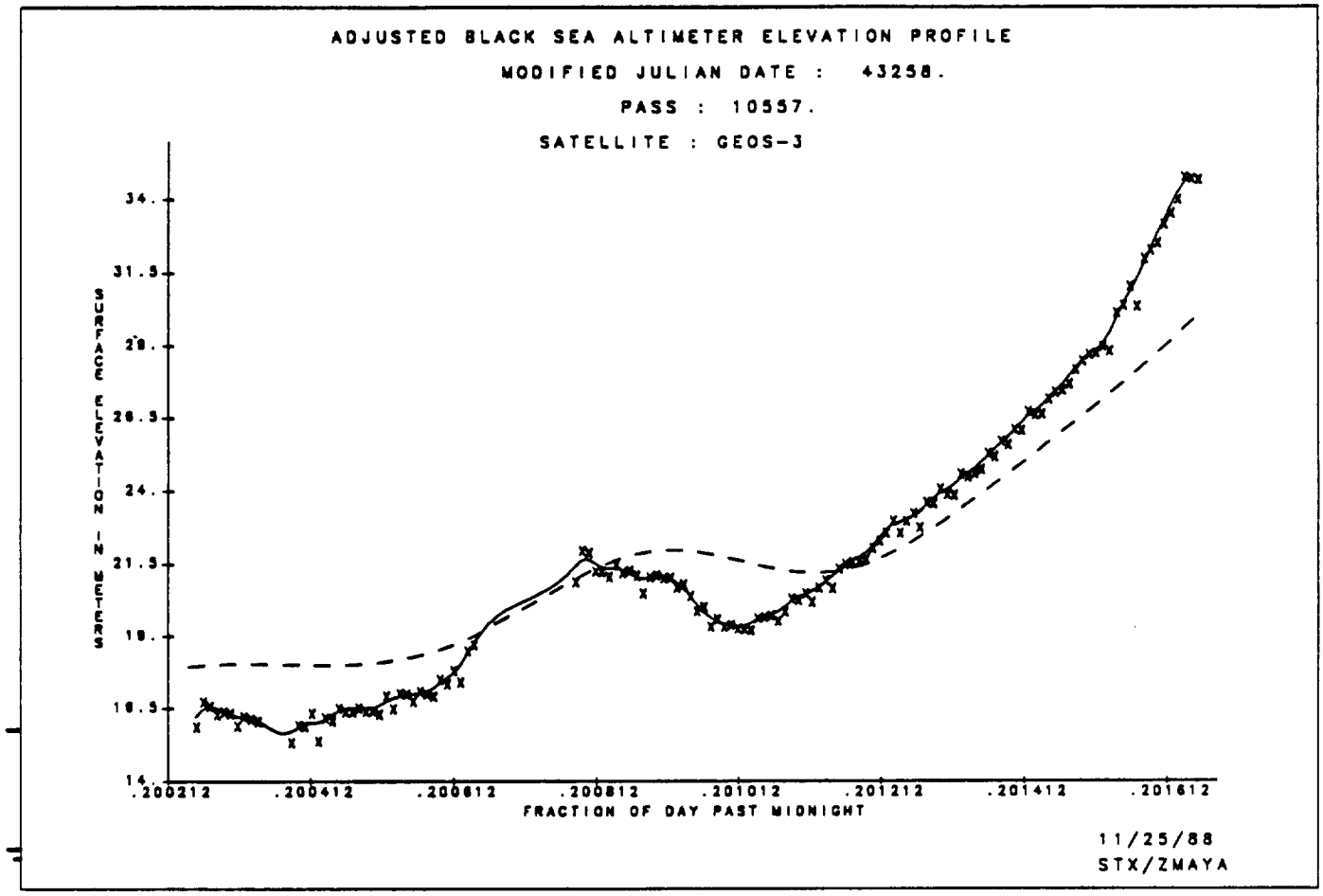

Figure 5a. Sample adjusted altimeter elevation profiles of the Black Sea. Rapp's 180 x 180 geoid model is represented by the dash curve.

Profile of the reference pass.

ORIGINAL PAGE IS
OF POOR QUALITY

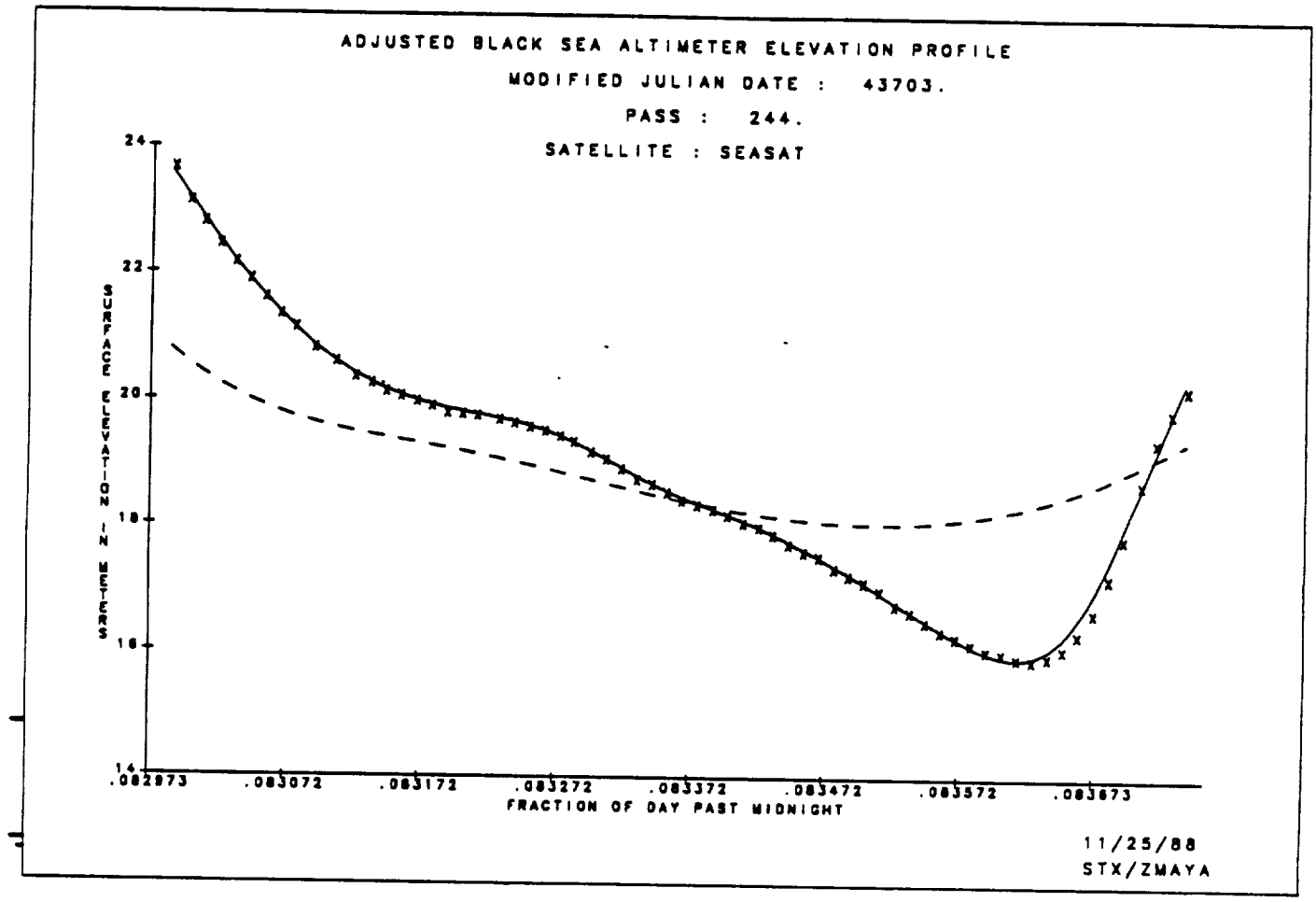

Figure 5b. Sample adjusted altimeter elevation profiles of the Black Sea. Rapp's 180 x 180 geoid model is represented by the dash curve.

Typical profile.

study, because it has been reprocessed into a consistent format that obscures the mode. However, Wagner (1979) found a total RMS of 33 cm in the high-frequency spectra from 47 passes of global and intensive GEOS-3 altimeter data. For the SEASAT data, Townsend (1980) reported a data noise level between 6 and 10 cm, with the higher values occurring at higher sea states.

The RMS of crossover differences consists of the square root of the mean of a weighted sum of squares of data of different precisions. If we assume that the data of the two crossing passes is uncorrelated, then the sum of squares is comprised of three terms:

1) twice the variance of GEOS-3 data, weighted by the number of GEOS-3 crossovers;
2) twice the variance of SEASAT data, weighted by the number of SEASAT crossovers;
3) the sum of variances of GEOS-3 and SEASAT data, weighted by the number of mixed crossovers.

If we insert the above satellite data variances into the above sum-of-squares equation, we may establish the reality of our observed crossover RMS. Inserting $[25\ cm]^2$ and $[10\ cm]^2$ for GEOS-3 and SEASAT variances, respectively, an RMS crossover difference of 0.28 m is predicted, which is in good agreement with our crossover RMS of 0.25 meters.

Over the Caspian Sea there are 1074 possible crossovers, 539 of which are GEOS-3 with GEOS-3, 79 are SEASAT with SEASAT and 456 are GEOS-3 with SEASAT. The crossover-cleanup process described above for the Black Sea was also applied to the Caspian Sea crossovers. Two passes that cross no other passes were removed from the dataset. This reduced the number of crossovers to 972, of which 494 are GEOS-3 with GEOS-3, 77 are SEASAT with SEASAT and 401 are GEOS-3 with SEASAT. The RMS of crossover differences before crossover adjustment is 2.21 m. The RMS after crossover adjustment is reduced to 37

cm. The reference pass is the SEASAT pass #832. Typical adjusted profiles and their corresponding reference models are shown in Figure 6.

Following the method described above, if we insert reported variances for data of one satellite into the expression for the RSS (residual-squared sum) of the Caspian Sea crossover differences, the resulting variance of the other satellite's data may be checked against reported precision values. If, for example, we insert a variance corresponding to 6 cm noise for SEASAT, we find that the corresponding GEOS-3 noise level satisfying the crossover RMS is 32 cm. If we insert a variance for SEASAT corresponding to a 10-cm noise level, the corresponding GEOS-3 noise level satisfying the crossover RMS is about 31 cm. Both of these numbers are quite reasonable according to the references cited above. On the other hand, if we insert a GEOS-3 noise level of 25 cm, we find that this implies a SEASAT noise level of 31 cm, which is unreasonably high, whereas inserting a GEOS-3 noise level of 50 cm is prohibited (requires square roots of negative numbers). Thus our crossover RMS of 0.38 meters is consistent with reasonable values of SEASAT and GEOS-3 altimeter precisions.

After the data were corrected for pass biases, an overall bias representing the average difference in height between the reference pass and the reference geoid is added to the data. For the Caspian Sea, the adjustment was -34 m, and for the Black Sea data, 0 m.

Preliminary Analysis of the Adjusted Data

The adjusted inland sea data must be gridded for geodetic collocation analyses. This is a time-consuming process unless the data records are properly arranged. To group data records by proximity to the same grid point, program SORT (Au *et al.*, 1989) reads through a dataset

ORIGINAL PAGE IS
OF POOR QUALITY

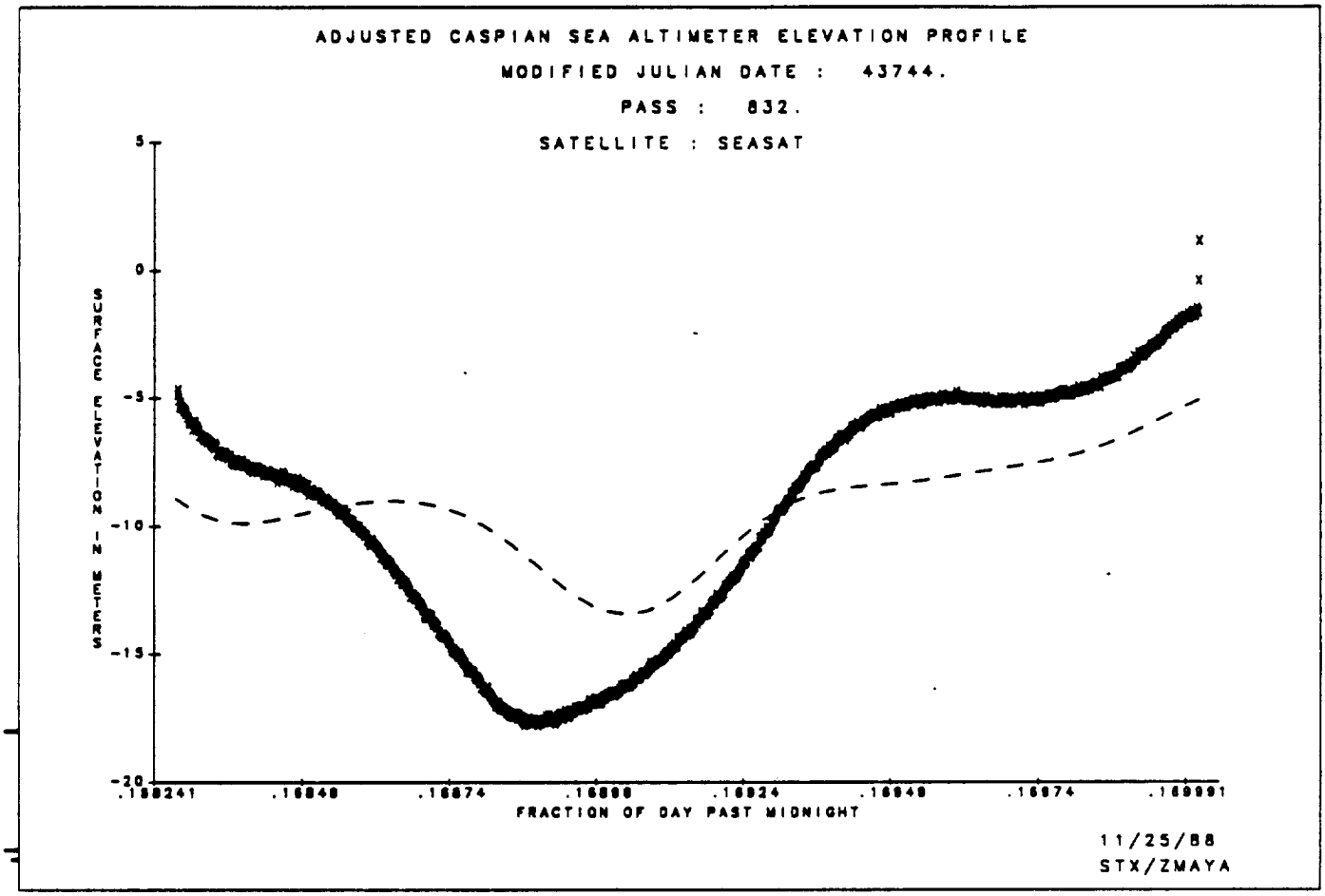

Figure 6a. Sample adjusted altimeter elevation profiles of the Caspian Sea. Rapp's 180 x 180 geoid model is represented by the dash curve.

Profile of the reference pass.

ORIGINAL PAGE IS
OF POOR QUALITY

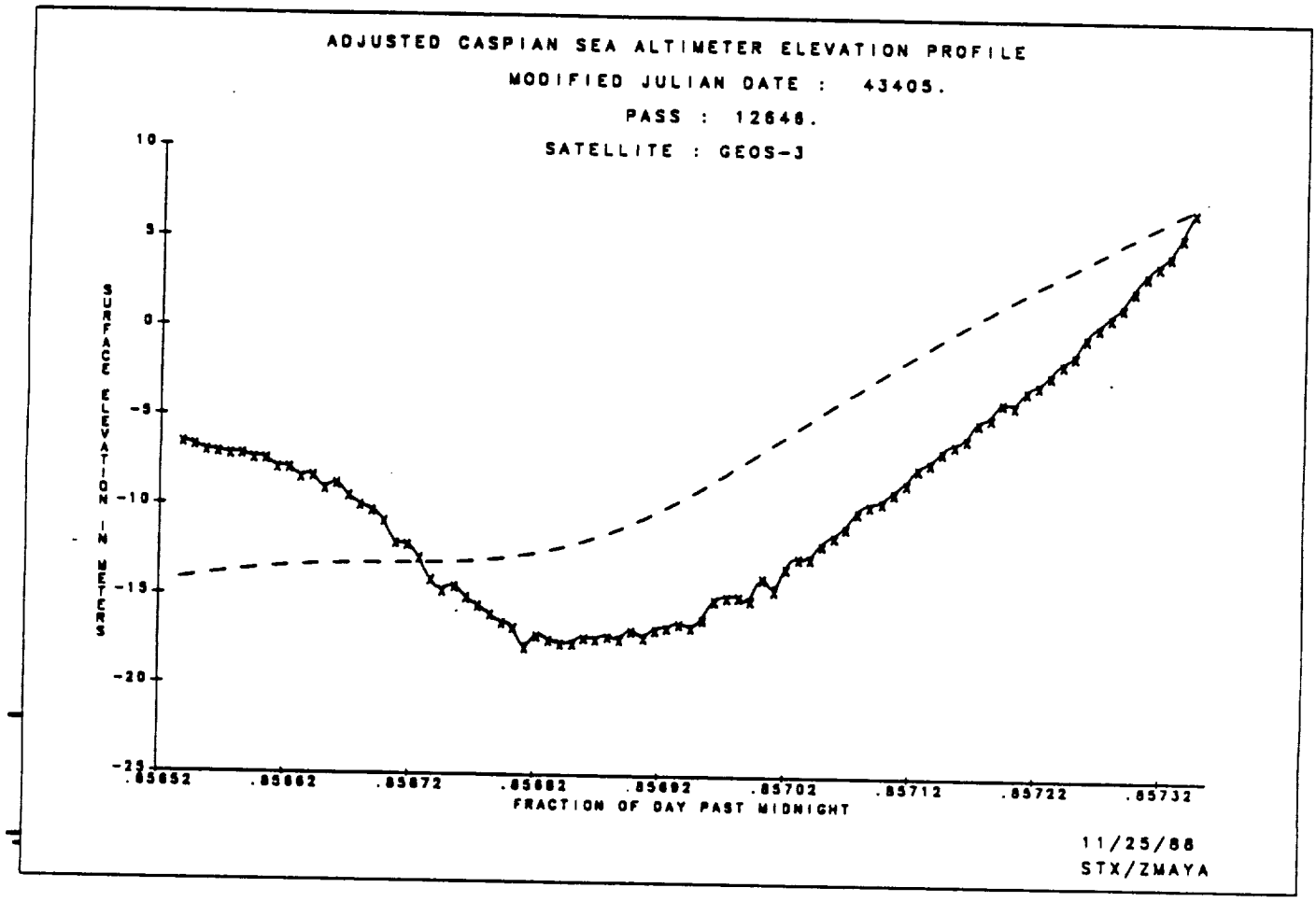

Figure 6b. Sample adjusted altimeter elevation profiles of the Caspian Sea. Rapp's 180 x 180 geoid model is represented by the dash curve.

Typical profile.

and determines the grid points, depending on the chosen cap size, with which a particular data record is associated. Identification indices are then assigned to each data record so that data records associated with a common grid point can be grouped together by a sort / merge process. In the current report, the grid size is a quarter degree. The cap radius chosen for subsequent data analyses is also a quarter degree, so that all data within a quarter degree of a given grid point are associated with that grid point. Note that it is possible for a given data record to be associated with as many as four grid points.

Geoid undulations of the inland seas were initially gridded according to the method of weighted averages using Program WGTAVG (Au *et al.*, 1989). The weight of a data point with respect to a grid point is a function of the square of its distance from the grid point. Contour maps of the weighted-average geoid undulations of the Black and Caspian Seas are shown in Figures 7 and 8, respectively. The contour maps of the geoid undulations of the Black Sea and Caspian Sea according to the reference geopotential model, Rapp's 180 x 180 model, are shown in Figures 9 and 10, respectively. Program CONTOUR (Au *et al.*, 1989) is used for contouring both the gridded data and reference models.

The contour maps of the weighted-average and reference geoid undulations of the Black Sea closely resemble each other. The geoid contour maps of the Caspian Sea, however, show substantial differences. Assuming comparable short-wavelength information content in the altimeter data over both seas, it can be concluded that there is more short-wavelength information in the reference geoid undulation model of the Black Sea than in the model of the Caspian Sea. The information content of a reference geopotential model has considerable effect on the quality of gravity anomaly results transformed from geoid undulation data, as will be shown in later sections.

ORIGINAL PAGE IS
OF POOR QUALITY

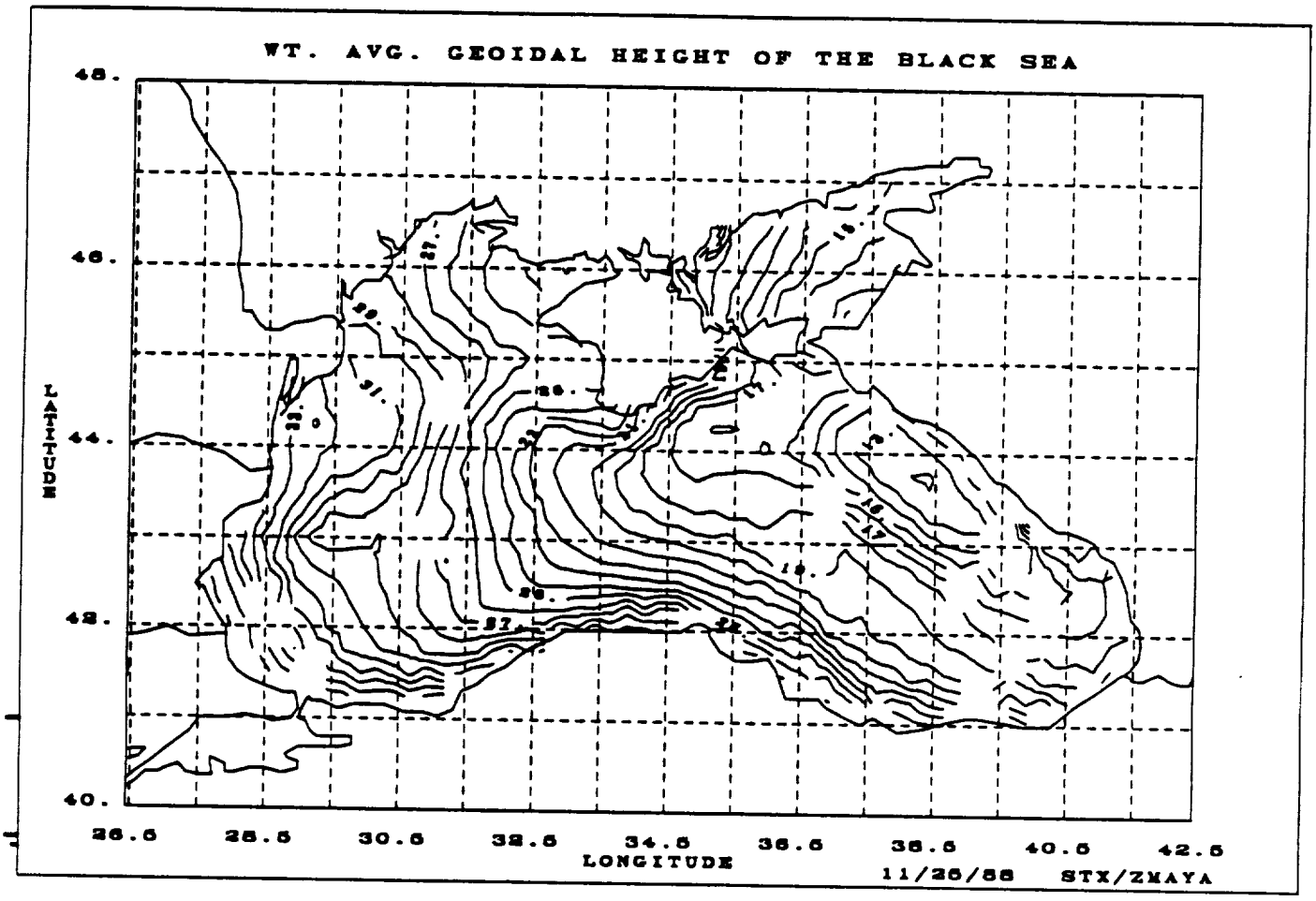

Figure 7. A contour map of the weighted-average geoid undulations (m above mean sea level) of the Black Sea.

ORIGINAL PAGE
OF POOR QUALITY

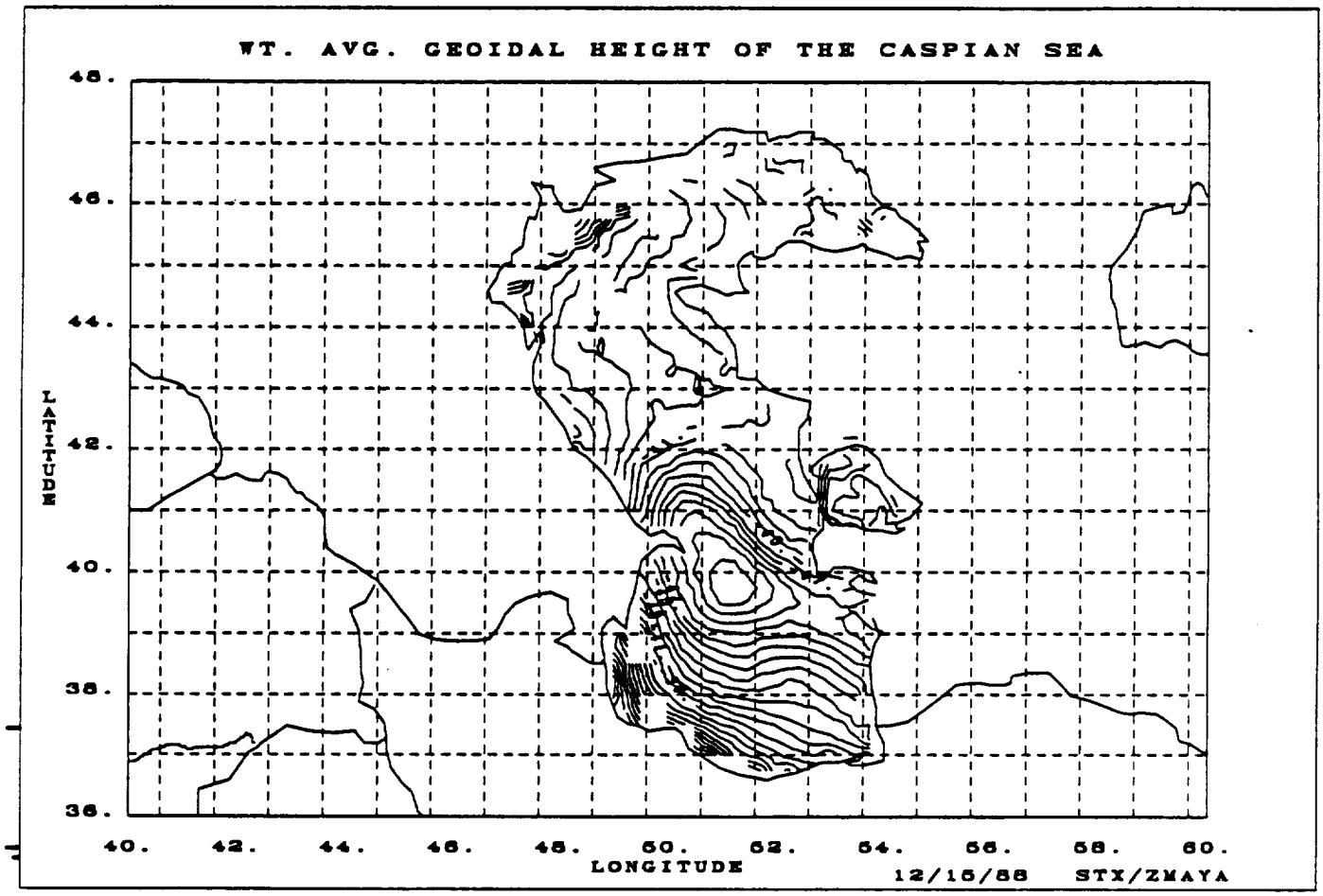

Figure 8. A contour map of the weighted-average geoid undulations (m above mean sea level) of the Caspian Sea.

ORIGINAL PAGE IS
OF POOR QUALITY

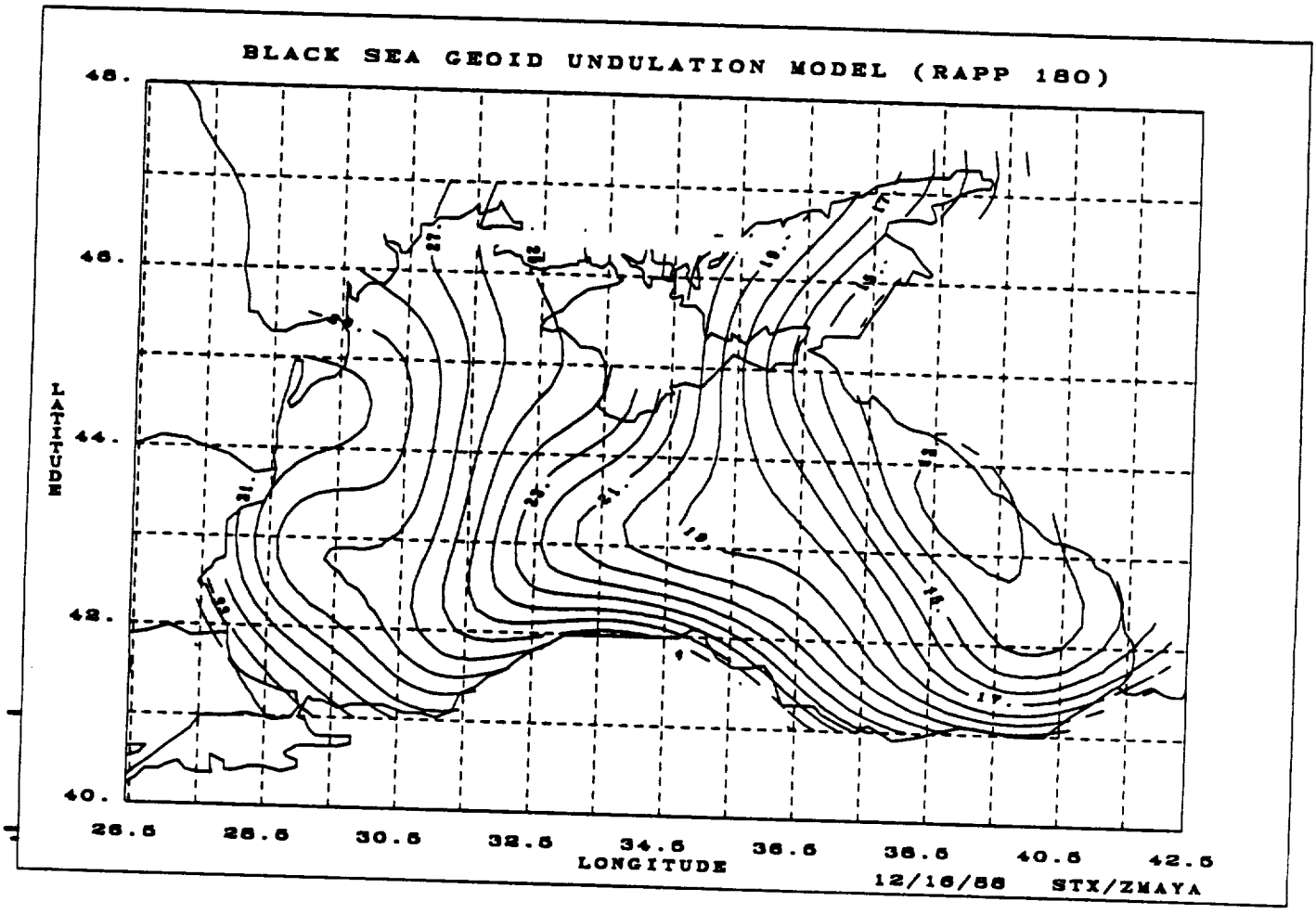

Figure 9. A contour map of Rapp's 180 x 180 reference geoid undulations (m above mean sea level) of the Black Sea.

ORIGINAL PAGE IS
OF POOR QUALITY

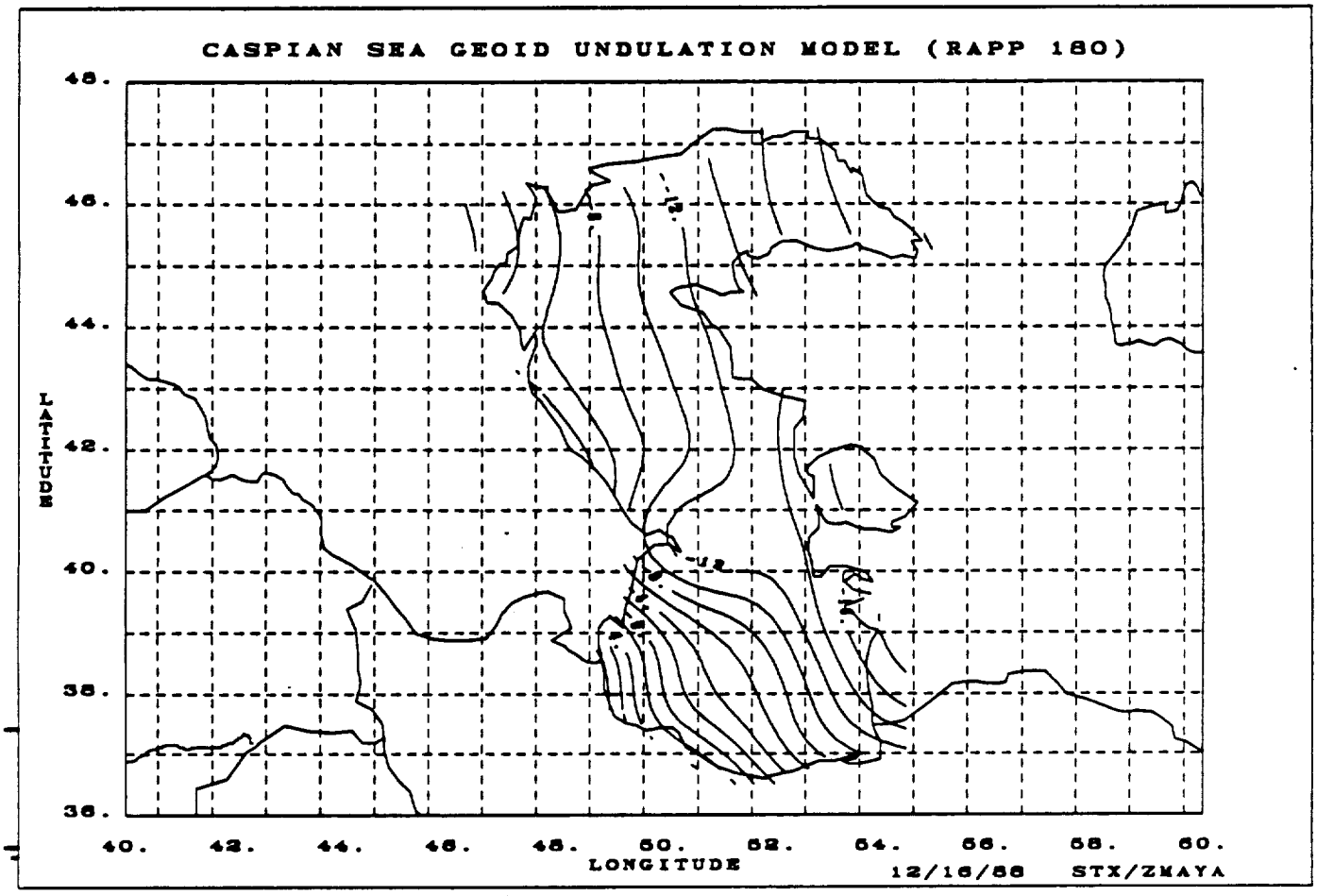

Figure 10. A contour map of Rapp's 180 x 180 reference geoid undulations (m above mean sea level) of the Caspian Sea.

III. BRIEF DESCRIPTION OF LINEAR LEAST-SQUARES INTERPOLATION AND COLLOCATION

Collocation is a predictive method based on linear least-squares interpolation. A general description of collocation can be found in Moritz (1978). A brief review of the collocation method is given in this section.

Let $f(P)$ be a predicted value of a function at a point P. The predicted value can be expressed by a linear combination of m observable (stochastic variables) in the neighborhood of P, such that

$$f(P) = \sum_{i=1}^{m} a_{Pi} N_{Pi}$$

$$= \alpha_P N_P \tag{5}$$

where N_P is an $m \times 1$ vector of observables and a_P is a set of nonunique coefficients. If T_P is the true value of the function at P, the local interpolation error ϵ_P at P is given by

$$\epsilon_P = T_P - \alpha_P N_P$$

$$= \{ \; 1 \quad -\alpha_P \; \} \begin{bmatrix} T_P \\ N_P \end{bmatrix} . \tag{6}$$

Similarly, interpolation error at another point Q is

$$\epsilon_Q = \{ \; 1 \quad -\alpha_Q \; \} \begin{bmatrix} T_Q \\ N_Q \end{bmatrix} . \tag{7}$$

The error covariance for points P and Q is

$$\epsilon_{PQ} \equiv \tilde{\epsilon_Q} \epsilon_P$$

$$= \{\ T_Q \quad \tilde{N}_Q\ \} \quad \begin{bmatrix} 1 \\ -a_Q \end{bmatrix} \quad \{\ 1 \quad -a_P\ \} \quad \begin{bmatrix} T_P \\ N_P \end{bmatrix}$$

$$= \{\ 1 \quad -a_P\ \} \quad \begin{bmatrix} T_P \\ N_P \end{bmatrix} \quad \{\ T_Q \quad \tilde{N}_Q\ \} \quad \begin{bmatrix} 1 \\ -a_Q \end{bmatrix} \quad . \tag{8}$$

Let M be an average operator such that

$$\sigma_{PQ} = M\{\epsilon_P \epsilon_Q\} \tag{9}$$

is the error covariance of prediction errors ϵ_P and ϵ_Q at points P and Q. A covariance matrix, Σ, can be defined as

$$\Sigma = M \left\{ \begin{bmatrix} T_P \\ N_P \end{bmatrix} \quad \{\ T_Q \quad \tilde{N}_Q\ \} \right\}$$

$$= \begin{bmatrix} C_{PQ} & \tilde{C}_{P\tilde{N}} \\ C_{NQ} & C_{N\tilde{N}} \end{bmatrix} \tag{10}$$

where C_{PQ} is the error covariance of points P and Q, $\tilde{C}_{P\tilde{N}}$ is an $n \times 1$ covariance vector relating the elements of N_Q to T_P, C_{NQ} is an $m \times 1$ covariance vector relating the elements of N_P to T_Q, and $C_{N\tilde{N}}$ is an $m \times n$ covariance matrix of the elements of N_P and N_Q. Elements of the covariance matrix are values of a chosen covariance function that reflect the interdependence of two observables. A covariance function, therefore, can be any mathematical function, e.g., an ensemble average of observables, or an empirical formula.

The error covariance of P and Q is then given by

$$\sigma_{PQ} = C_{PQ} - a_Q C_{PN} - a_P C_{QN} + a_P C_{N\tilde{N}} a_P \tag{11}$$

and the variance at P is

$$\sigma_P^2 = C_o - 2a_P C_{PN} + a_P C_{N\tilde{N}} a_P \tag{12}$$

where C_o is the assumed error at the prediction point P.

The necessary condition for a minimum of σ_P^2 is that

$$\partial \sigma_P^2 / \partial a_P = 0 \tag{13}$$

which implies that

$$a_P = (C_{N\tilde{N}})^{-1} C_{PN} \quad . \tag{14}$$

Substituting a_P into the equations for $f(P)$ and for the variance at P, the predicted value at P and its variance are given by

$$f(P) = C_{PN}(C_{N\tilde{N}})^{-1} N_P \tag{15}$$

$$\sigma_P^2 = C_{PP} - \tilde{C}_{PN}(C_{N\tilde{N}})^{-1} C_{PN} \quad . \tag{16}$$

The covariance matrix previously derived is only for the stochastic variables. If there are random errors associated with the stochastic variables, the stochastic covariance matrix should be supplemented by an error covariance matrix $D_{N\tilde{N}}$, such that

$$C_{\ell\ell} = C_{N\tilde{N}} + D_{N\tilde{N}} \tag{17}$$

is the covariance matrix. The predicted value at P becomes

$$f(P) = \tilde{C}_{PN} C_{\ell\ell}^{-1} N_P \tag{18}$$

where C_{PN} remains unchanged. The notation that indicates a transpose, $\tilde{}$, will be omitted in the following sections.

IV. APPLICATION OF COLLOCATION TECHNIQUE

Collocation Gridding of Geoid Undulations

According to the linear least-squares interpolation formula, the predicted geoid undulation $N(P)$ at a point P is given by

$$N(P) = C_{PN}(C_{NN})^{-1}N_P \tag{19}$$

where C_{PN} is a covariance vector relating the undulation at P to the observable in the neighborhood of P, and C_{NN} is the covariance matrix. The covariance matrix is the sum of the stochastic covariance matrix and the error covariance matrix. In the current report, the error covariance matrix is a combination of the random error associated with each observable and the error covariance matrix obtained from crossover adjustments. The stochastic covariance matrix is derived from a local residual covariance function based on the difference between gridded weighted-average geoid undulations and the reference geopotential model. A convolution technique described by Moritz (1978) is used to determine the local covariance function. The local covariance function is constructed by convolution of the difference between the weighted-average geoid data and the reference geoid. The resultant covariance function is, in effect, a least-squares filter (Treitel and Robinson, 1966). This filter determines the contribution of each observable to the predicted value at a grid point. It is observed that the interpolation results are rather insensitive to the covariance function being used as long as reasonable effective weights are assigned to each observable. For example, if the weights are assigned as a function of the inverse of the square of distance from the point at which prediction is made, the weighted-average results coincide with the collocation results.

The variance at each gridded point is given by

$$\sigma^2 = C_o - C_{PN}(C_{NN})^{-1}C_{PN} \qquad (20)$$

where C_o is the assumed value of the covariance function at the predicted point.

Program GEOID (Au *et al.*, 1989) was used to perform the geoid undulation interpolation, and Program EMPCOV (Au *et al.*, 1989) was used to determine local empirical covariance functions. The input dataset used in Program GEOID is a sorted version of the output from Program SORT, in which cutoff cap size is set to one quarter degree. The effective integration cap size of this interpolation is, therefore, also a quarter degree. The integration cap radius effectively excludes longer wavelength information from the gridding.

Contour maps of the geoid undulations of the Black and Caspian Seas gridded by the collocation method are shown, respectively, in Figures 11 and 12. The square root of the variance of the gridded data of the Black and Caspian Seas are plotted, respectively, in Figures 13 and 14. Note that this error in the gridded data varies inversely with the density of ground tracks (Figures 3 and 4) and is much smaller (10-cm RMS) for the Black Sea than for the Caspian Sea (20-cm RMS). This disparity in error values reflects somewhat the larger crossover error in the Caspian, but mostly the less uniform and sparser data distribution. Plots of the Black Sea and Caspian Sea local empirical covariance function are shown in Figures 15 and 16, respectively. Note that the weighted-average and collocation geoid undulation maps are very similar, demonstrating that collocation, when used as an interpolator, is not sensitive to the choice of covariance function.

ORIGINAL PAGE IS
OF POOR QUALITY

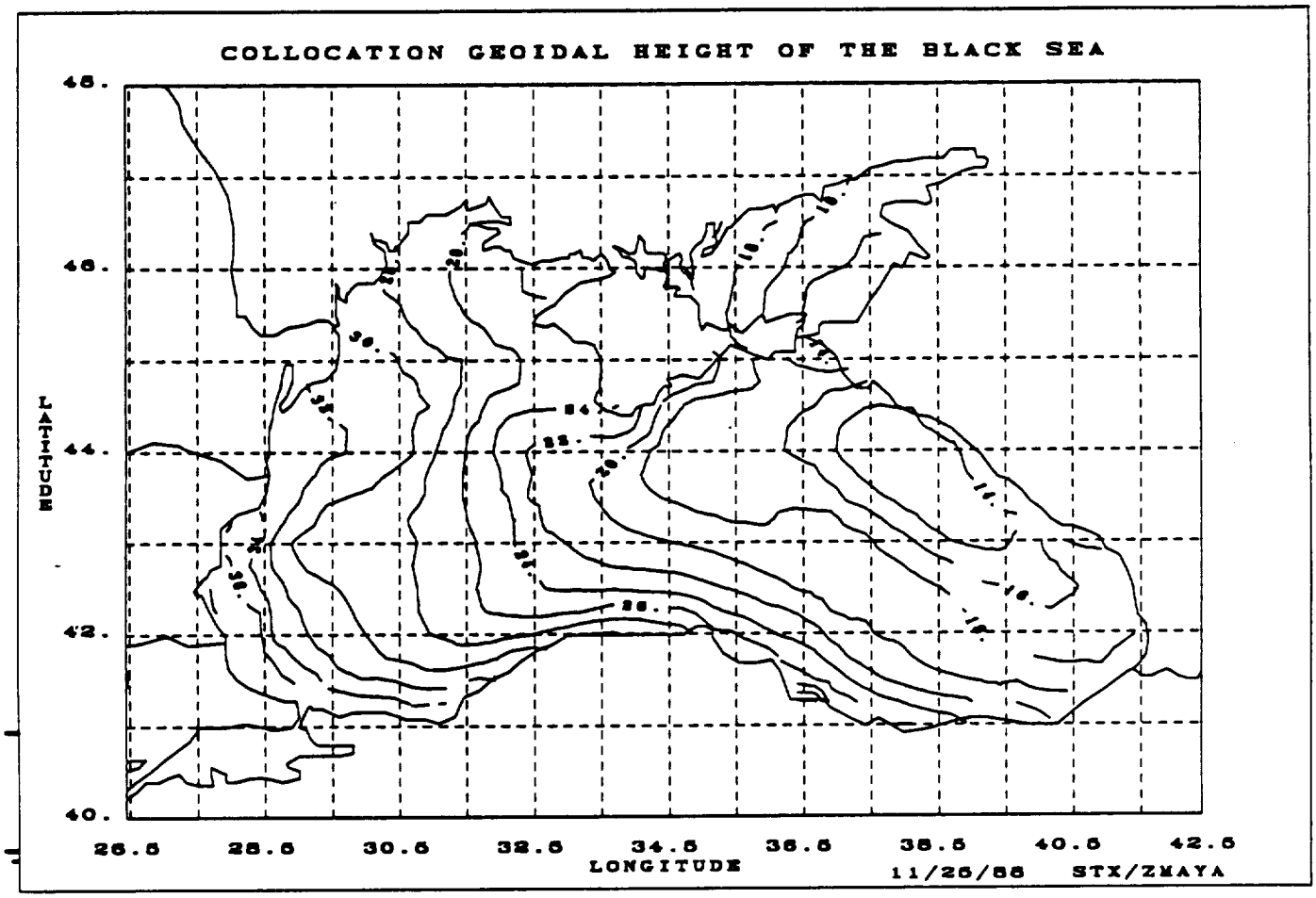

Figure 11. A contour map of the collocation geoid undulations (m above mean sea level) of the Black Sea.

ORIGINAL PAGE IS
OF POOR QUALITY

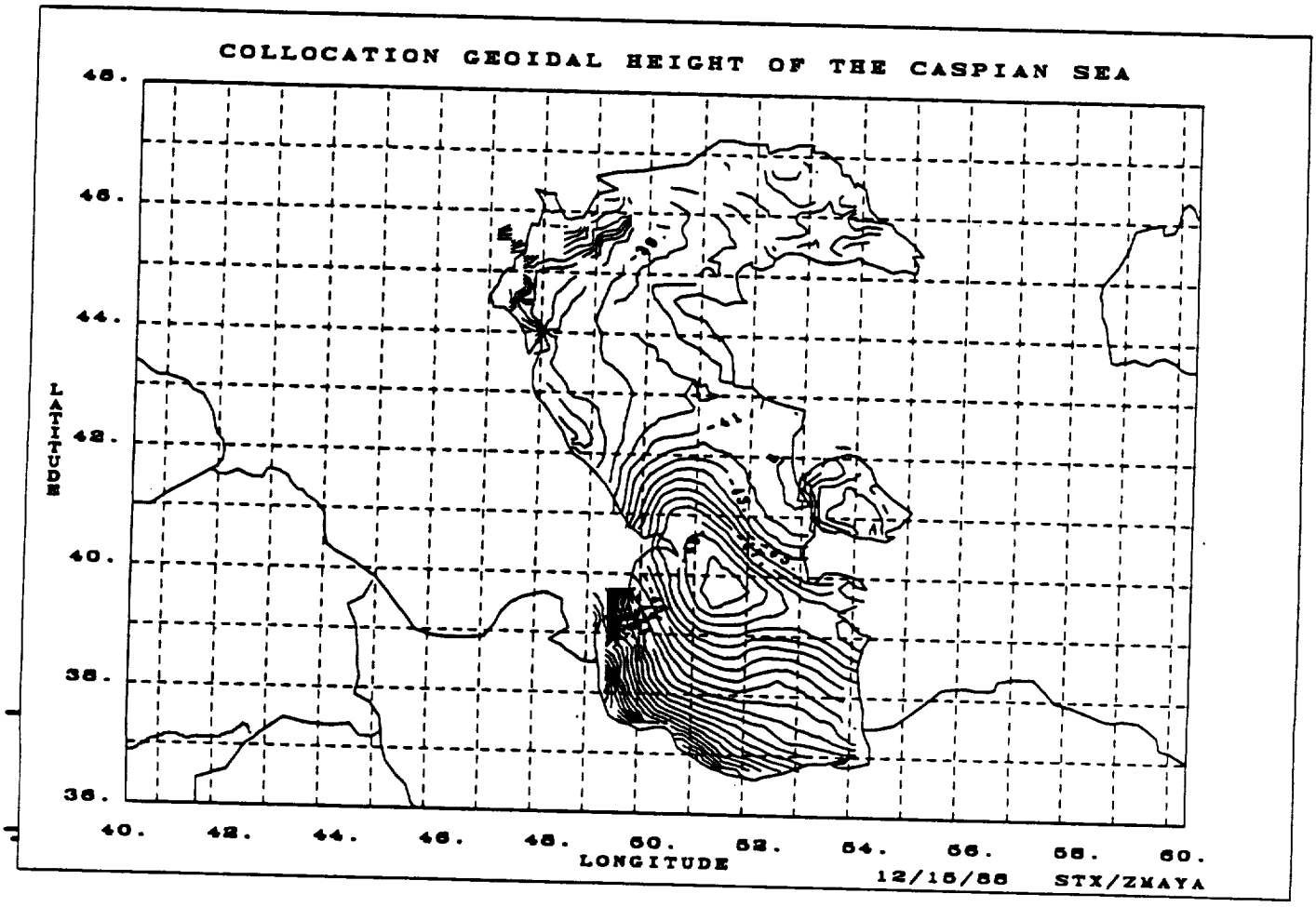

Figure 12. A contour map of the collocation geoid undulations (m above mean sea level) of the Caspian Sea.

ORIGINAL PAGE IS
OF POOR QUALITY

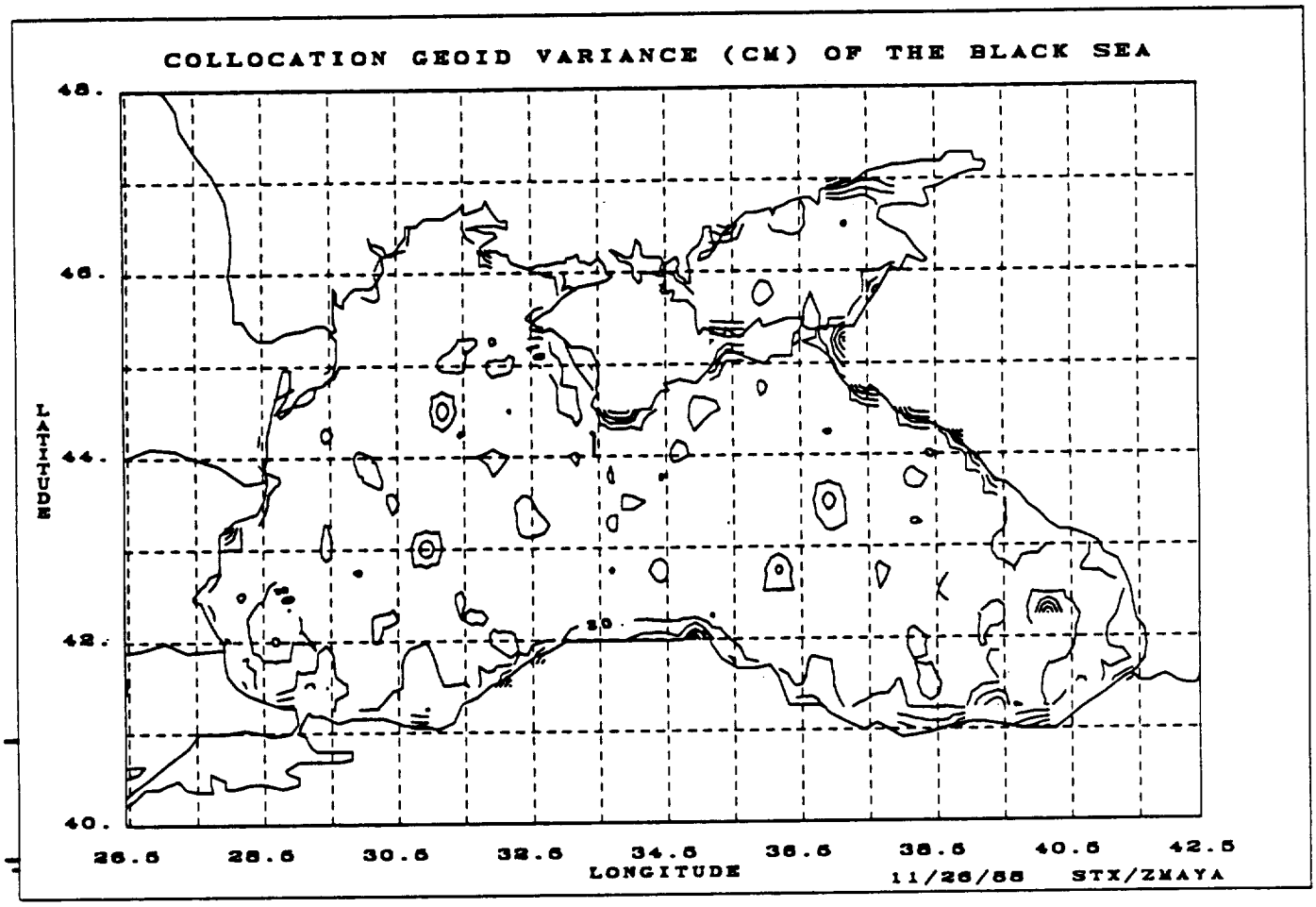

Figure 13. A contour map of the square root of the variance (cm) of the collocation geoid undulations of the Black Sea.

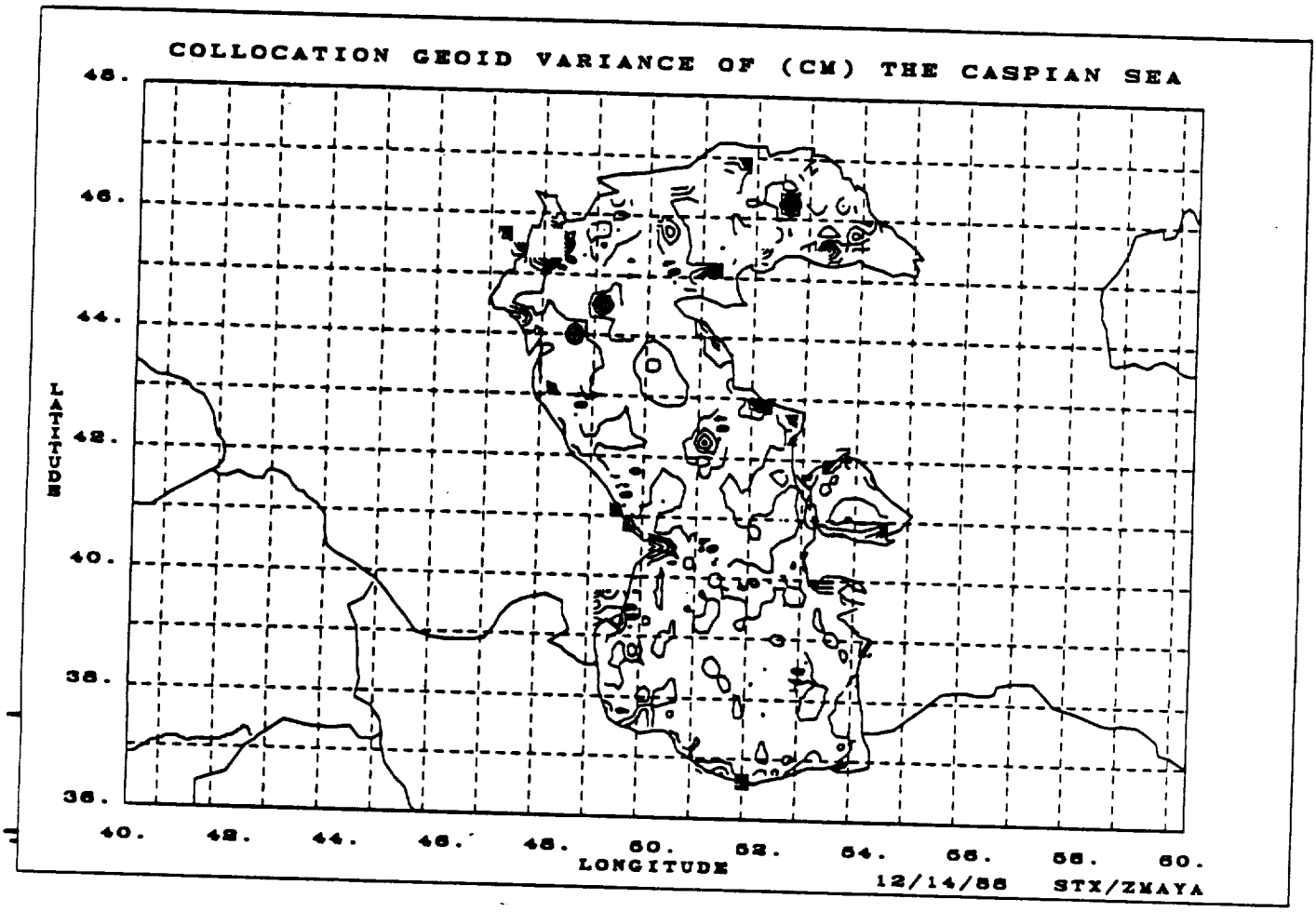

Figure 14. A contour map of the square root of the variance (cm) of the collocation geoid undulations of the Caspian Sea.

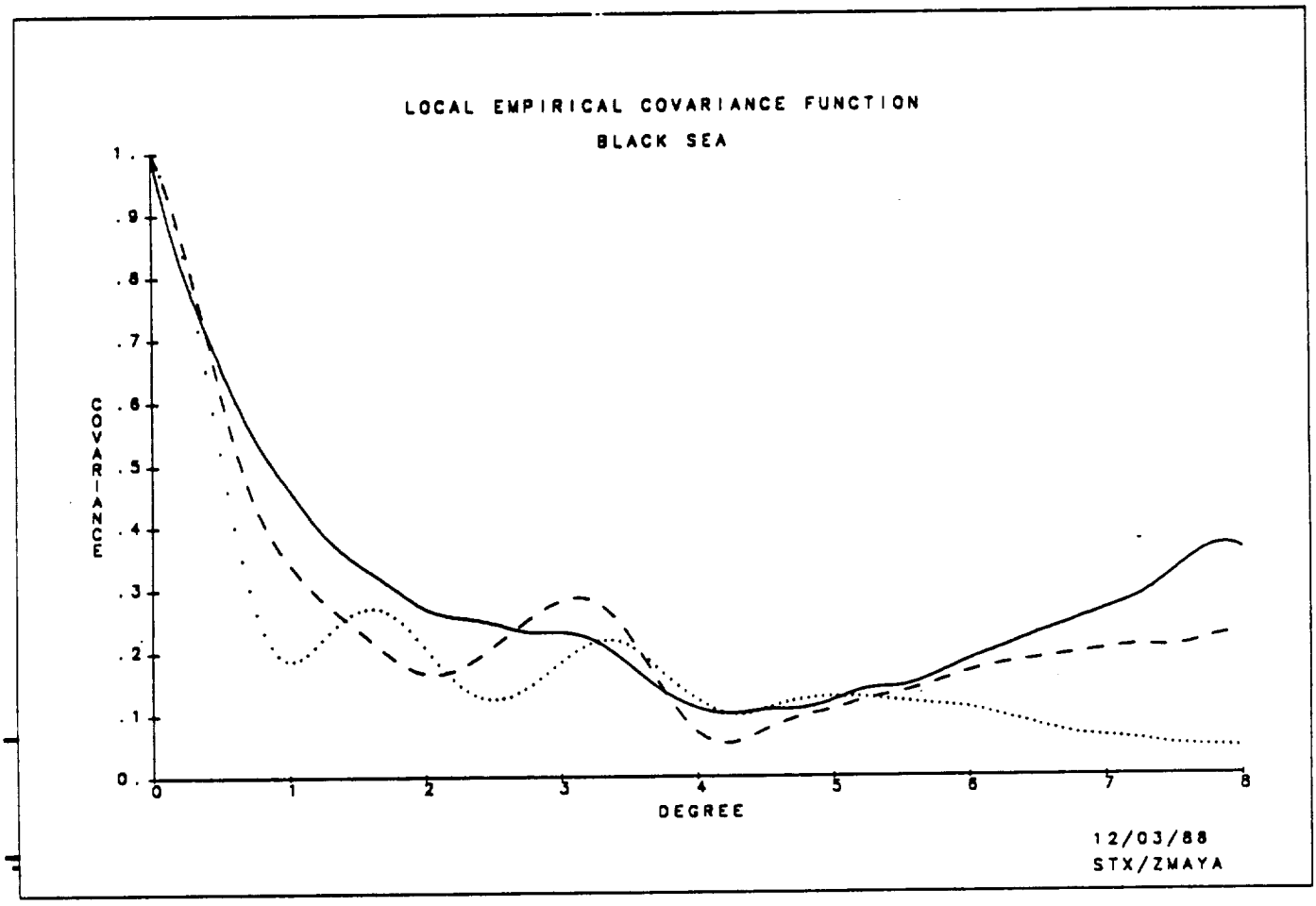

Figure 15. Normalized local residual empirical covariance functions of the Black Sea.

The normalization coefficients for:

1) undulation-undulation (solid line) is 1.61 m^2,

2) undulation-gravity (dash line) is 10.00 m-mgal, and

3) gravity-gravity (dotted line) is 125.5 $(mgal)^2$.

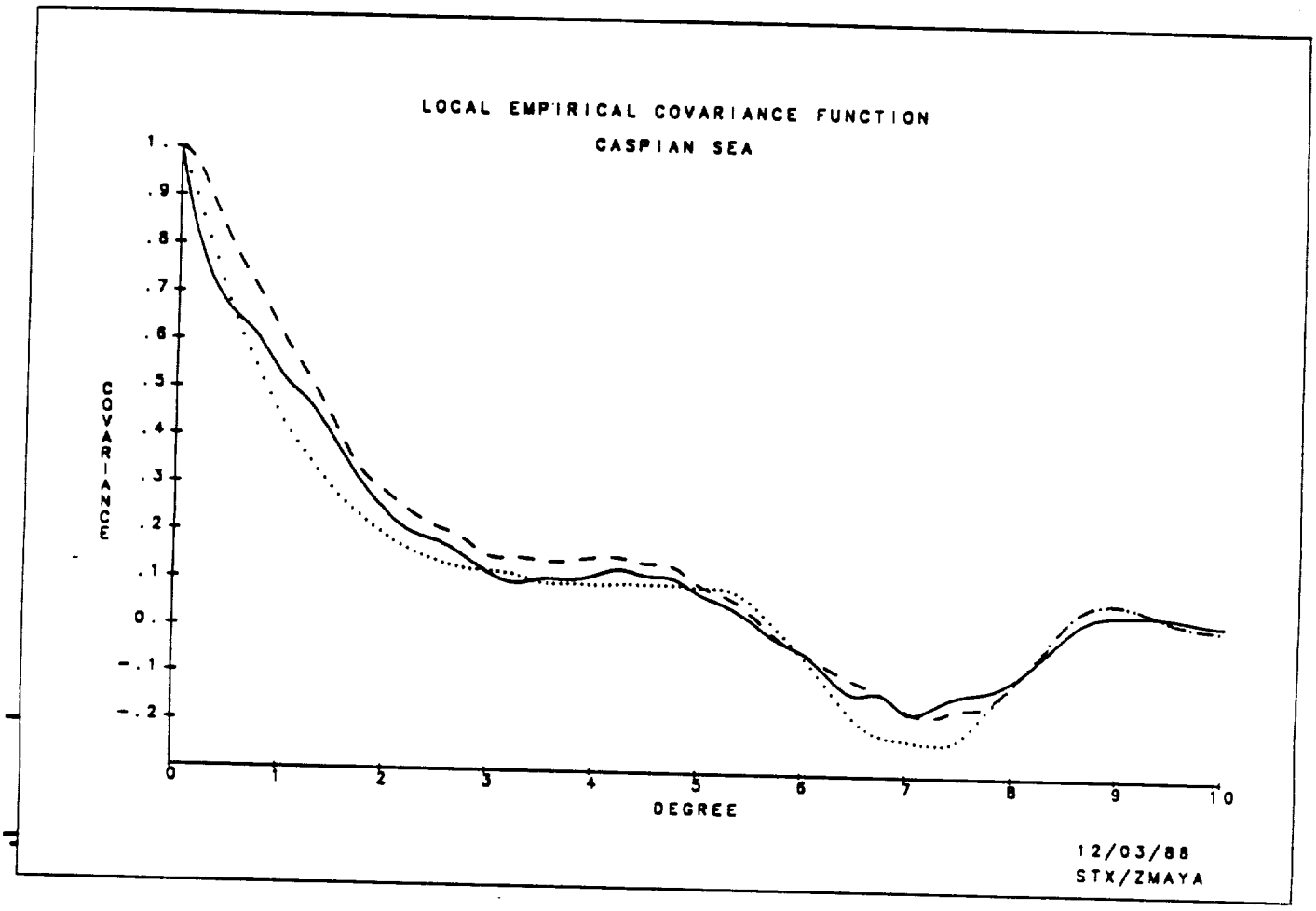

Figure 16. Normalized local residual empirical covariance functions of the Caspian Sea. The normalization coefficients for:

1) undulation-undulation (solid line) is 8.48 m^2,
2) undulation-gravity (dash line) is 42.15 m-mgal, and
3) gravity-gravity (dotted line) is 340.2 $(mgal)^2$.

Estimation of Gravity Anomalies

Following the collocation method described above, geoid undulations can be transformed into gravity anomalies (Rapp, 1986) according to the equation

$$\Delta g = C_{gN}(C_{NN}+D)^{-1}(N-N_R) + \Delta g_R \tag{21}$$

where Δg is the predicted point gravity anomaly, C_{gN} is the covariance vector of geoid-to-gravity transformation, C_{NN} is the covariance matrix for undulation-undulation interpolation, D is the error covariance matrix that is constructed in part from the variance of the previous interpolation of geoid undulations, N is the vector of gridded geoid undulations, N_R is the vector of reference model geoid undulations that corresponds to each observed value of N, and Δg_R is the reference model gravity anomaly value at the predicted grid point. The variance is given by

$$\sigma^2 = C_{gg} - C_{gN}(C_{NN}+D)^{-1}C_{gN} \tag{22}$$

where C_{gg} is the assumed value of the covariance function at the predicted grid point. Program GRAVAN (Au *et al.*, 1989) was used to perform the geoid-to-gravity transformation. The geoid undulations, gridded by collocation technique, and the corresponding variances, were used as input datasets. The demand for computer resources was greatly reduced by the choice of gridded data because a gridded dataset contains far fewer data points than an ungridded dataset.

In the current study, three sets of covariance functions were investigated for the undulation-to-gravity transformation. They are: 1) Rapp's empirical covariance functions based on a 180 x 180 global geopotential model, 2) theoretical self-consistent covariance functions (Jordan, 1972), and 3) local residual empirical covariance functions derived from iterative use

of the convolution method previously described. In some cases, it was necessary to augment the *a-priori* error matrix D in order to achieve stability in the gravity prediction. For the local empirical covariance functions, $[60\ cm]^2$ of variance was added to the diagonal of D, whereas for the Rapp and Jordan models, only $[25\ cm]^2$ of variance was added.

Plots of Rapp's 180 x 180 global covariance functions are shown in Figure 17. Contour maps of the estimated Black Sea gravity anomalies and the square root of their variance, using Rapp's covariance functions, are shown, respectively, in Figures 18 and 19. Corresponding results for the Caspian Sea, again using Rapp's covariance functions, are shown in Figures 20 and 21. As with the gridded geoid undulation error, the pattern of gravity anomaly error correlates inversely to the data distribution, but the magnitude of error is nearly the same at about 6 mgal RMS for both areas. For comparison, contour maps of the Black and Caspian Sea gravity anomalies derived from Rapp's 180 x 180 geopotential reference model are shown in Figures 22 and 23, respectively. Note the close agreement between reference and estimated gravity anomalies in the Black Sea, in contrast to the Caspian Sea results.

Initial estimates of 0.5° x 0.5° gravity anomalies in the Caspian Sea from point geoid data on a 0.25° grid were disappointing. The covariance functions were those used in the previous study, developed by Rapp from his 180 x 180 gravity reference field. Not only did the estimated gravity field look very different from the reference field, despite the close resemblance between the geoid height data and the reference model geoid, but, subsequent inverse collocation from gravity anomalies to geoid heights did not reproduce the gridded geoid heights. The previous study's estimates of gravity anomalies also appear to be very different from those of the reference field model.

A review of the literature for covariance functions indicated that the correlation distance

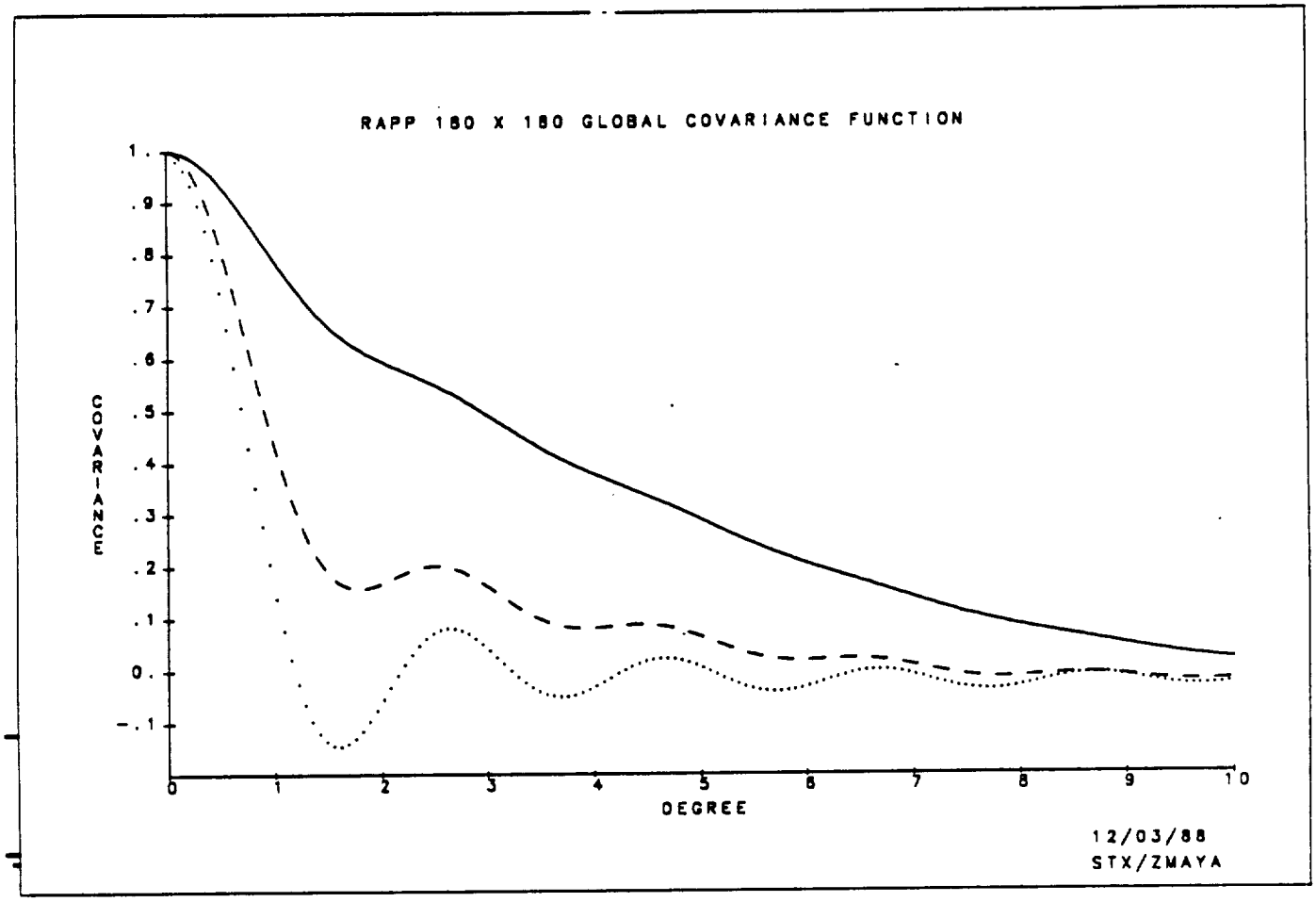

Figure 17. Normalized Rapp's 180 x 180 global covariance functions.

The normalization coefficients for:

1) undulation-undulation (solid line) is 1.13 m^2,

2) undulation-gravity (dash line) is 7.26 m-mgal, and

3) gravity-gravity (dotted line) is 98.36 $(mgal)^2$.

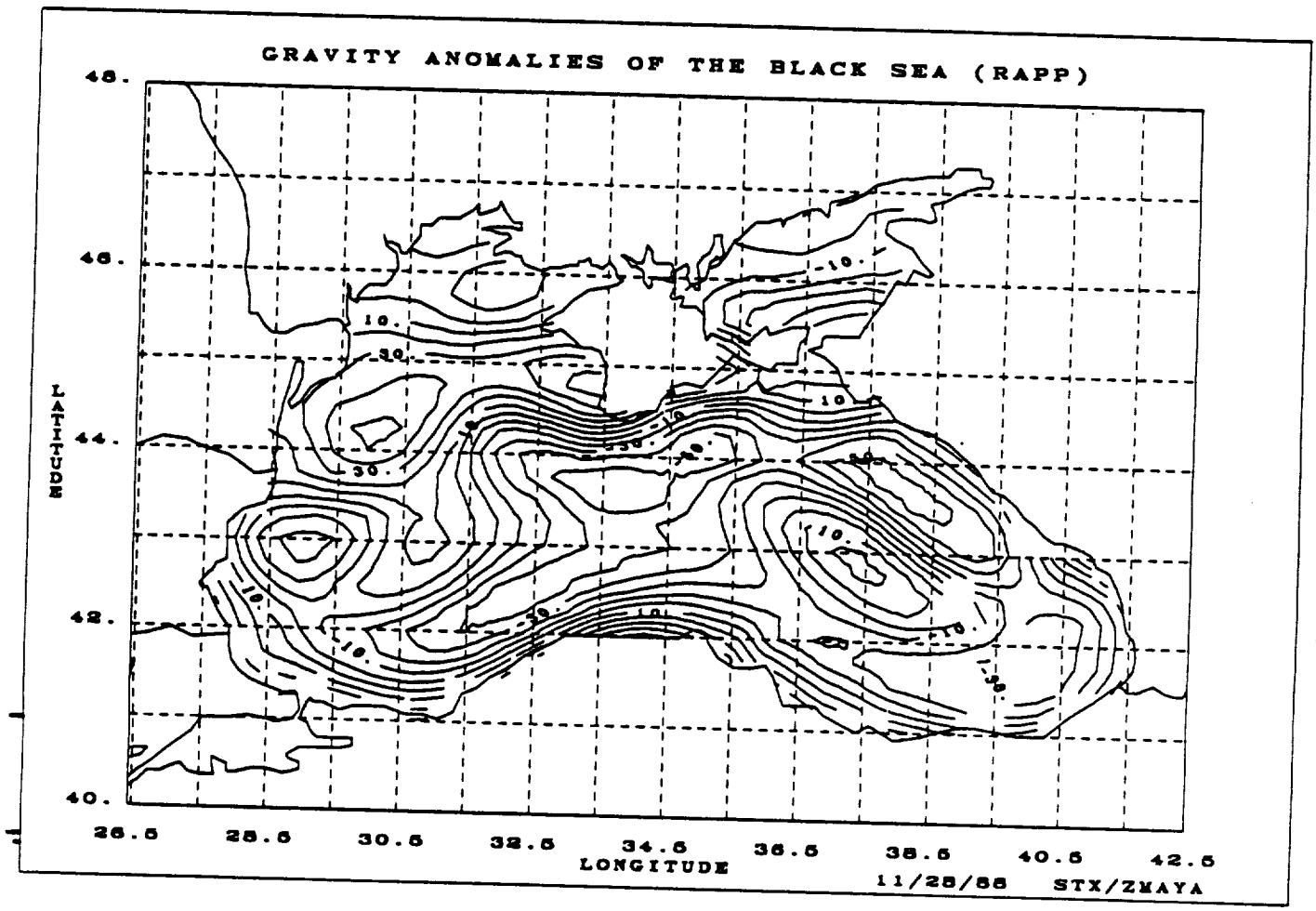

Figure 18. A contour map of estimated gravity anomalies (mgal) of the Black Sea based on Rapp's 180 x 180 global covariance functions.

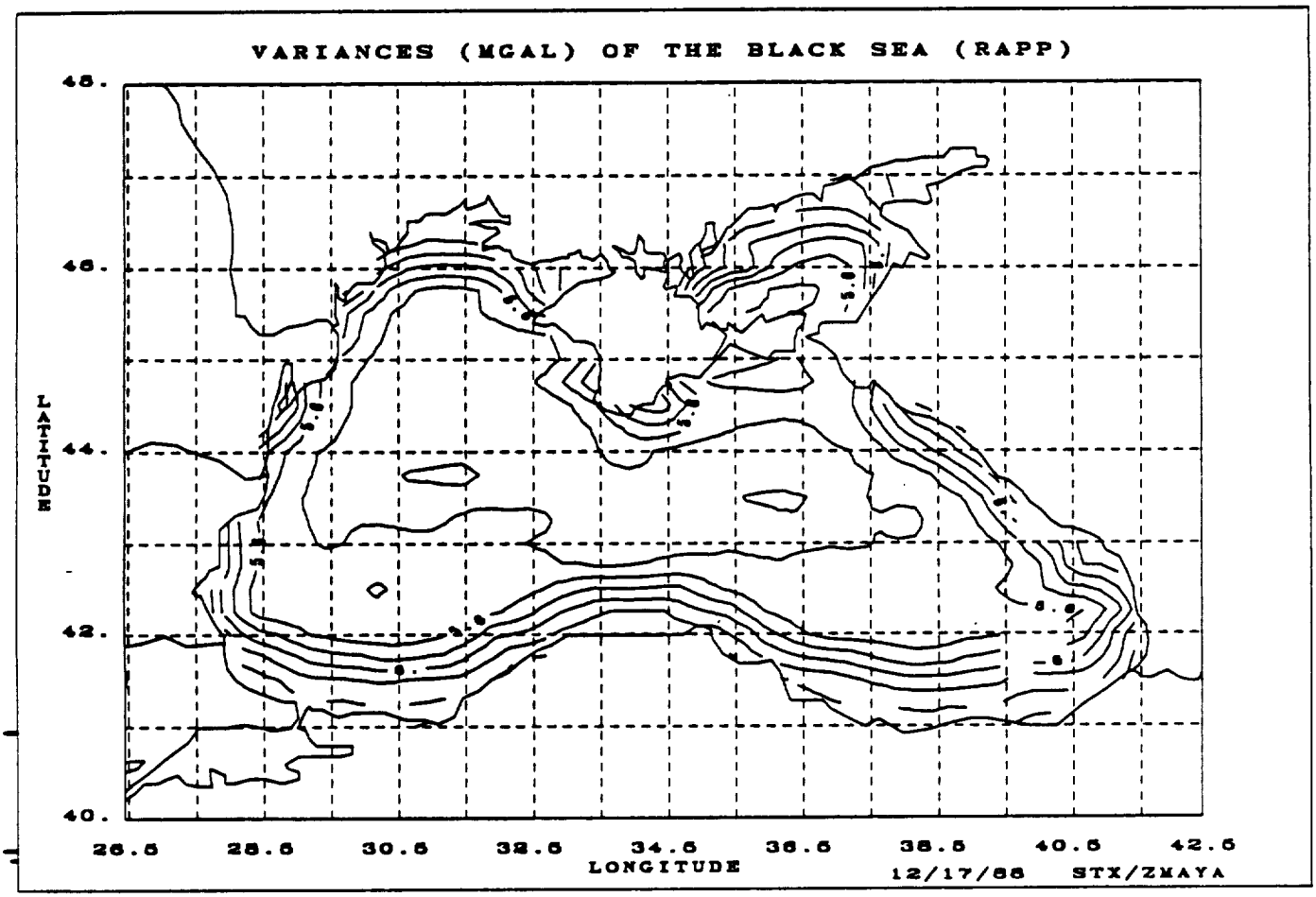

Figure 19. A contour map of the square root of the variances (mgal) of the estimated Black Sea gravity anomalies based on Rapp's 180 x 180 global covariance functions.

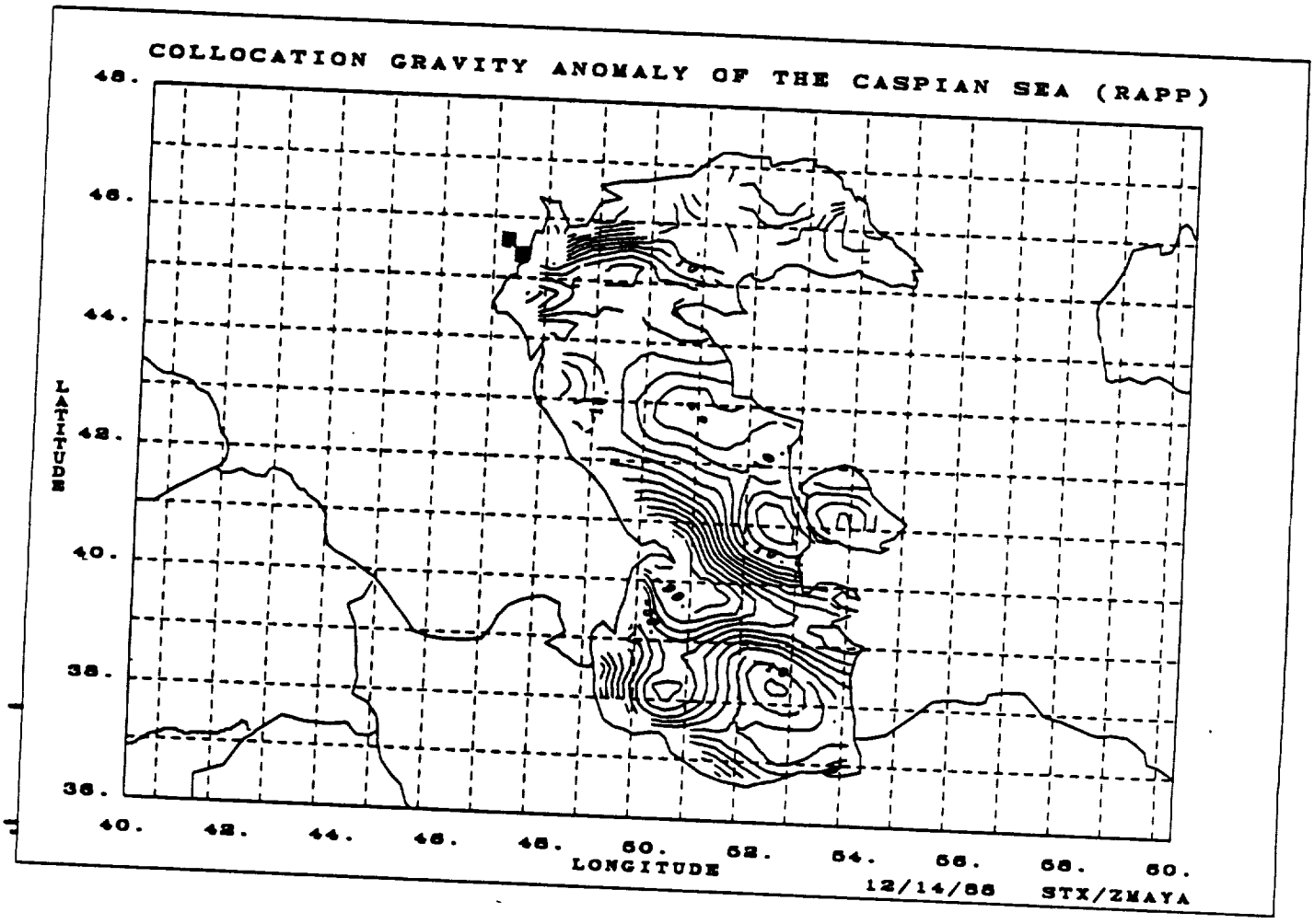

Figure 20. A contour map of estimated gravity anomalies (mgal) of the Caspian Sea based on Rapp's 180 x 180 global covariance functions.

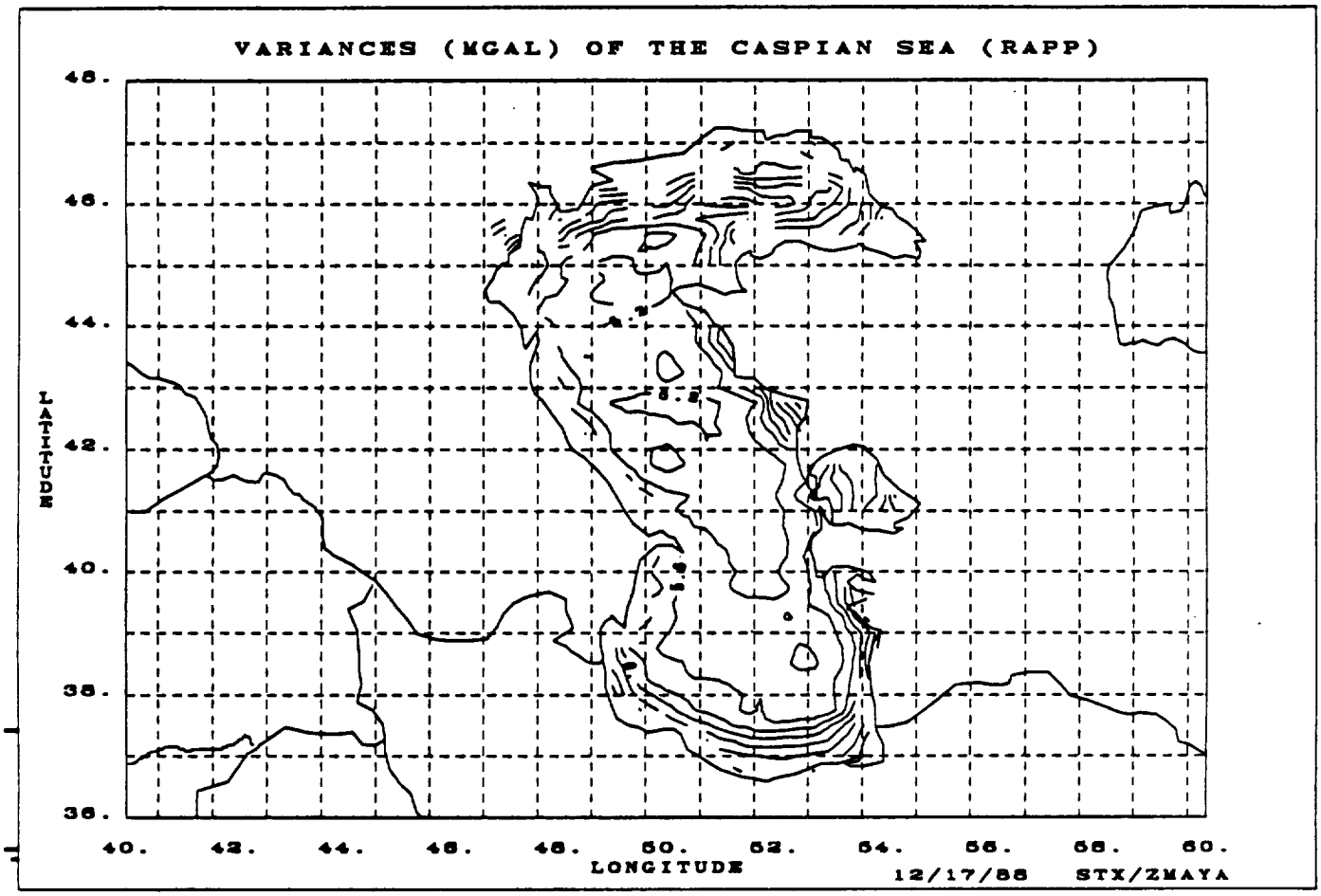

Figure 21. A contour map of the square root of the variances (mgal) of the estimated Caspian Sea gravity anomalies based on Rapp's 180 x 180 global covariance functions.

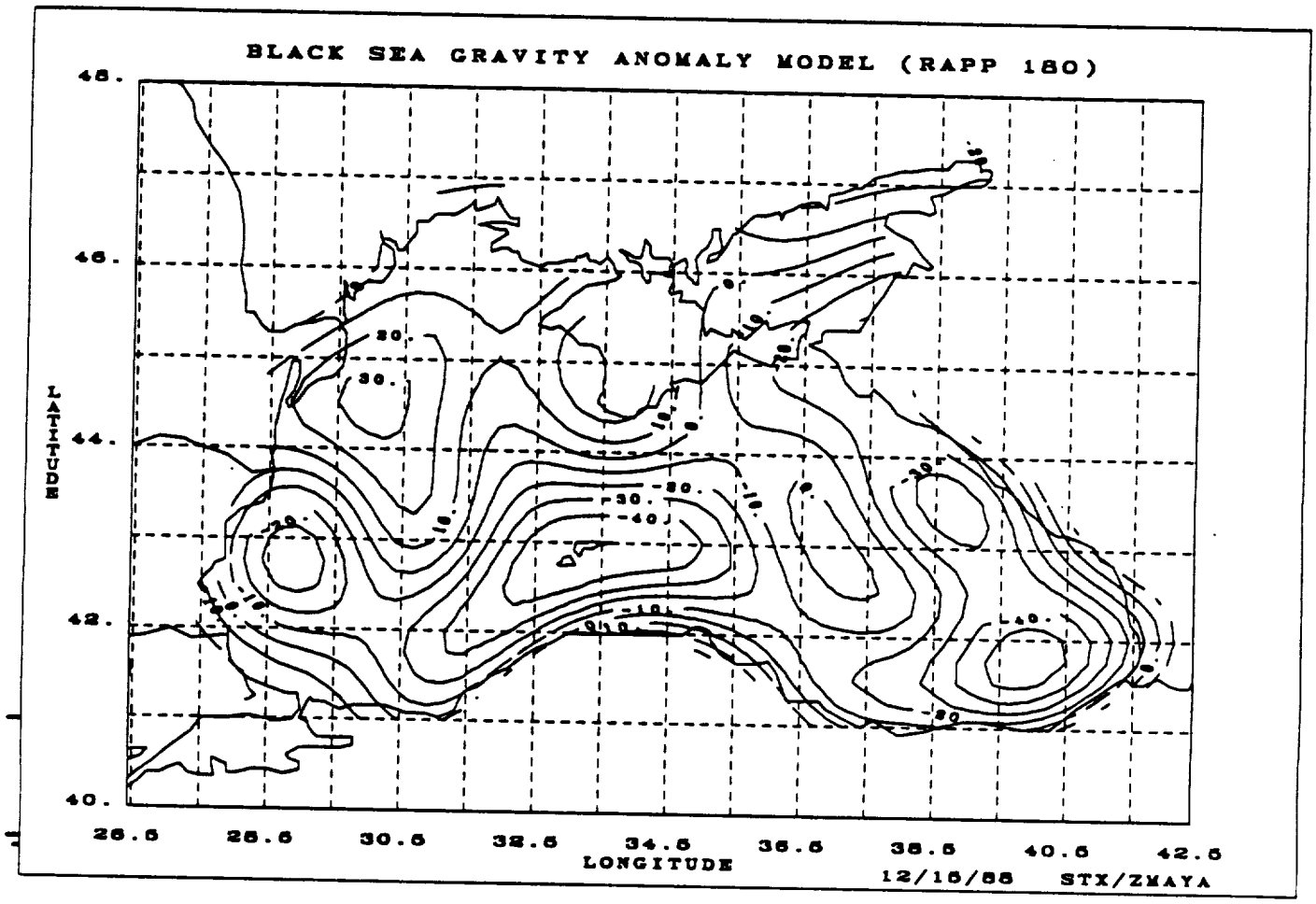

Figure 22. A contour map of Rapp's 180 x 180 reference gravity anomalies (mgal) of the Black Sea.

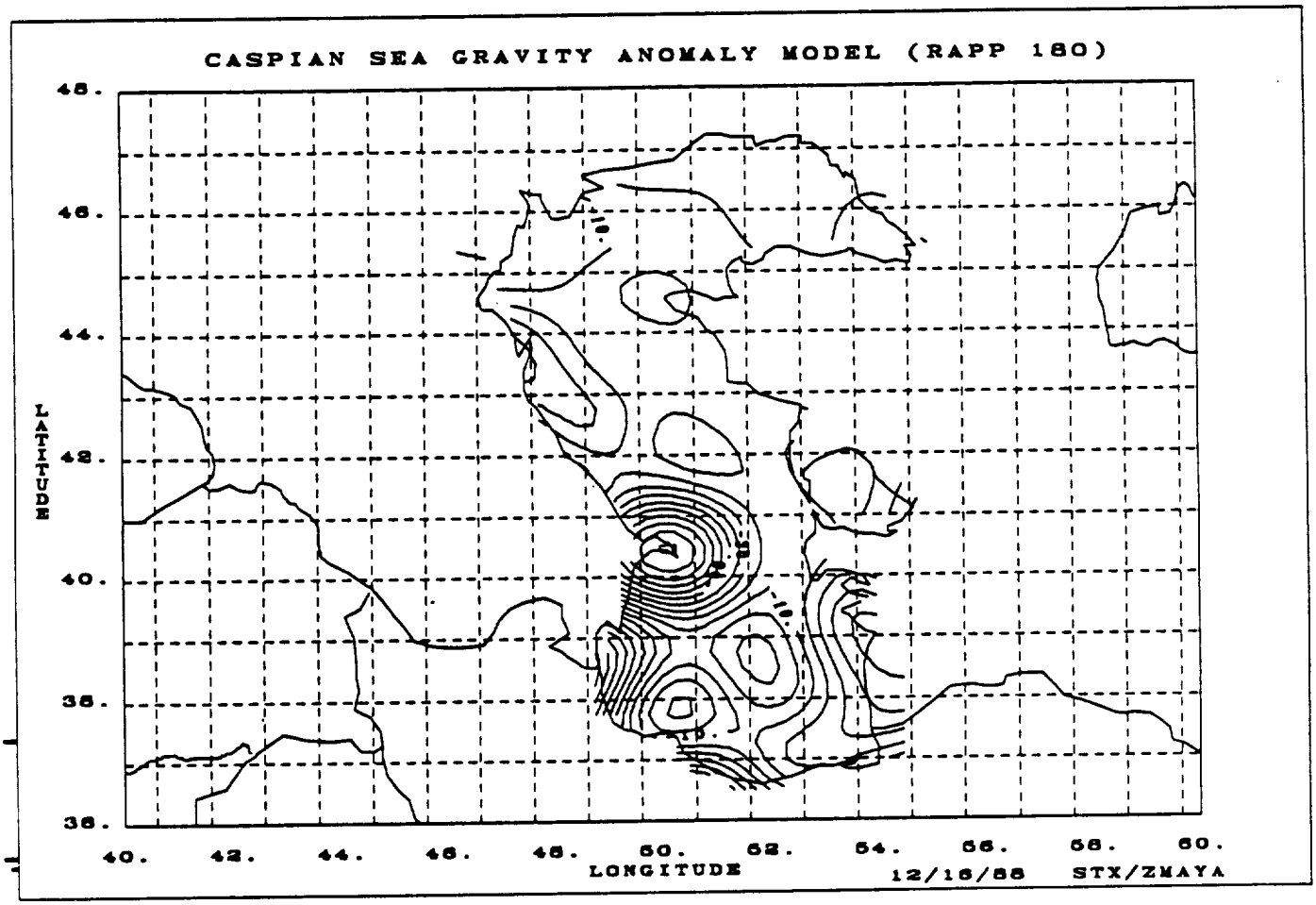

Figure 23. A contour map of Rapp's 180 x 180 reference gravity anomalies (mgal) of the Caspian Sea.

of Rapp's geoid undulation covariance function is much too long at 3 arc degrees. Models by Knudsen (1987) and by Jordan indicated a correlation distance for the geoid beyond degree 180 of 0.33 and 0.45 arc degrees, respectively. Correlation distance parameters for the gravity covariance function and the cross-covariance function also appeared too long, but not by so great a factor. As a trial, Jordan's self-consistent set of covariance functions was used, setting the geoid function correlation length to 0.5 arc-degree, with the result that the estimated gravity anomalies have a closer resemblance to the reference gravity model, and the inverse transformation yielded the original geoid.

Two parameters, C_0 and a correlation length, L, are required to calculate Jordan's covariance function. Both C_0 and L for the undulation-undulation case can be obtained from the local empirical covariance function derived from the weighted-average results. We have, however, no *a-priori* observed gravity anomaly data. A self-consistent approach to estimate the Jordan geoid-gravity and gravity-gravity covariance functions would be to empirically compute a covariance function from gravity anomalies predicted using Rapp's covariance functions. Local empirical covariance functions for the gravity-gravity case can be constructed to yield the required C_0 and correlation length, L, for Jordan's covariance functions. Program JORDAN (Au *et al.*, 1989) was used to determine consistent sets of Jordan's covariance functions. Plots of Jordan's covariance function for the Black Sea are shown in Figure 24. Contour maps of the predicted gravity anomalies and square root of the variance for the Black Sea are shown in Figures 25 and 26. Note that the predicted gravity error using the Jordan covariance function is slightly, but systematically smaller than that of the Rapp covariance function in Figure 19. The Jordan covariance functions for the Caspian Sea are shown in Figure 27; whereas results for the Caspian Sea are shown in Figures 28 and 29. In this case, Jordan's covariance function yields a predicted gravity error that is systematically and significantly

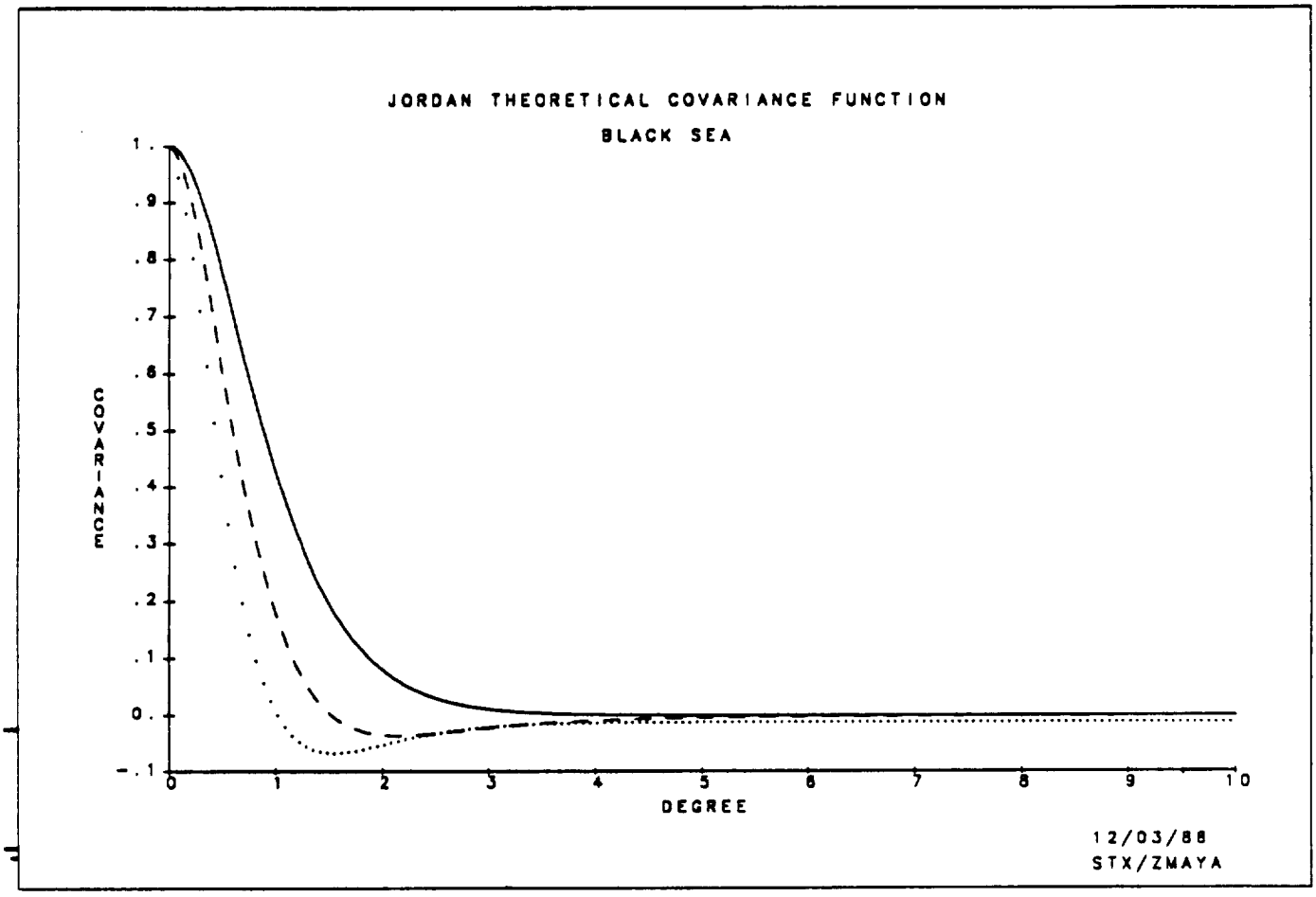

Figure 24. Normalized Jordan's theoretical covariance functions of the Black Sea.

The normalization coefficients for:

1) undulation-undulation (solid line) is 1.61 m^2,
2) undulation-gravity (dash line) is 11.61 m-mgal, and
3) gravity-gravity (dotted line) is 125.44 $(mgal)^2$.

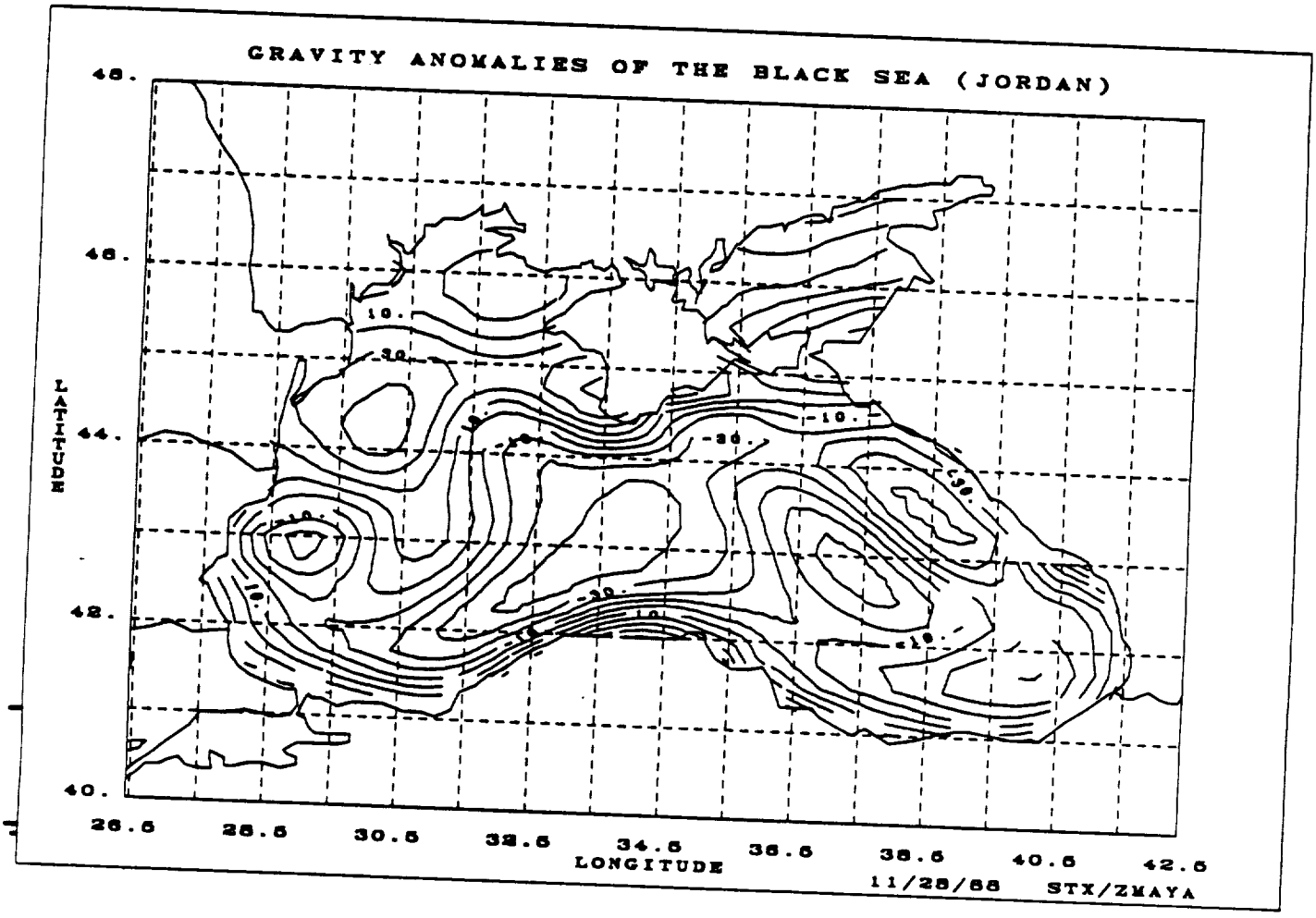

Figure 25. A contour map of estimated gravity anomalies (mgal) of the Black Sea based on Jordan's theoretical covariance functions.

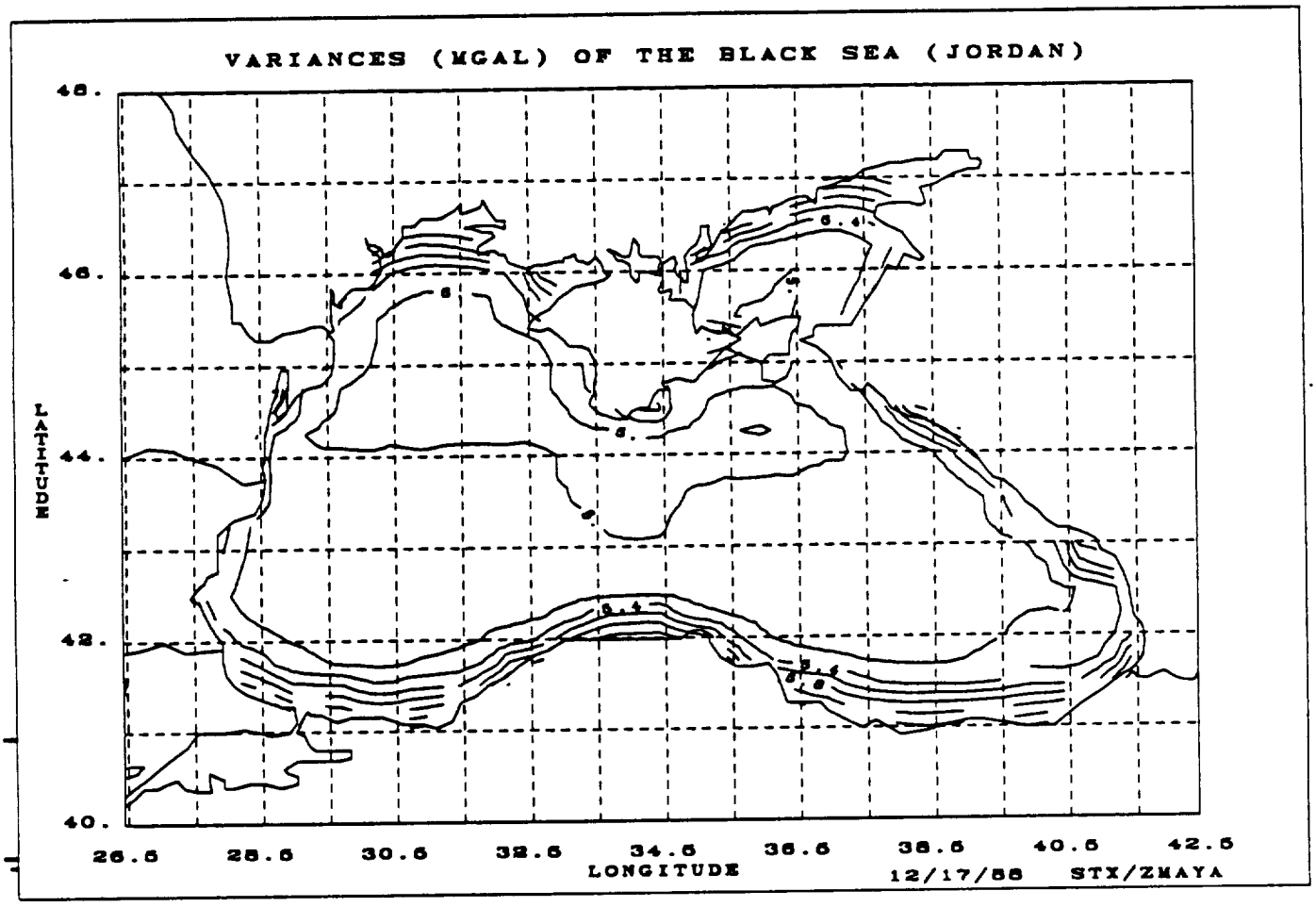

Figure 26. A contour map of the square root of the variances (mgal) of the estimated gravity anomalies of the Black Sea based on Jordan's theoretical covariance functions.

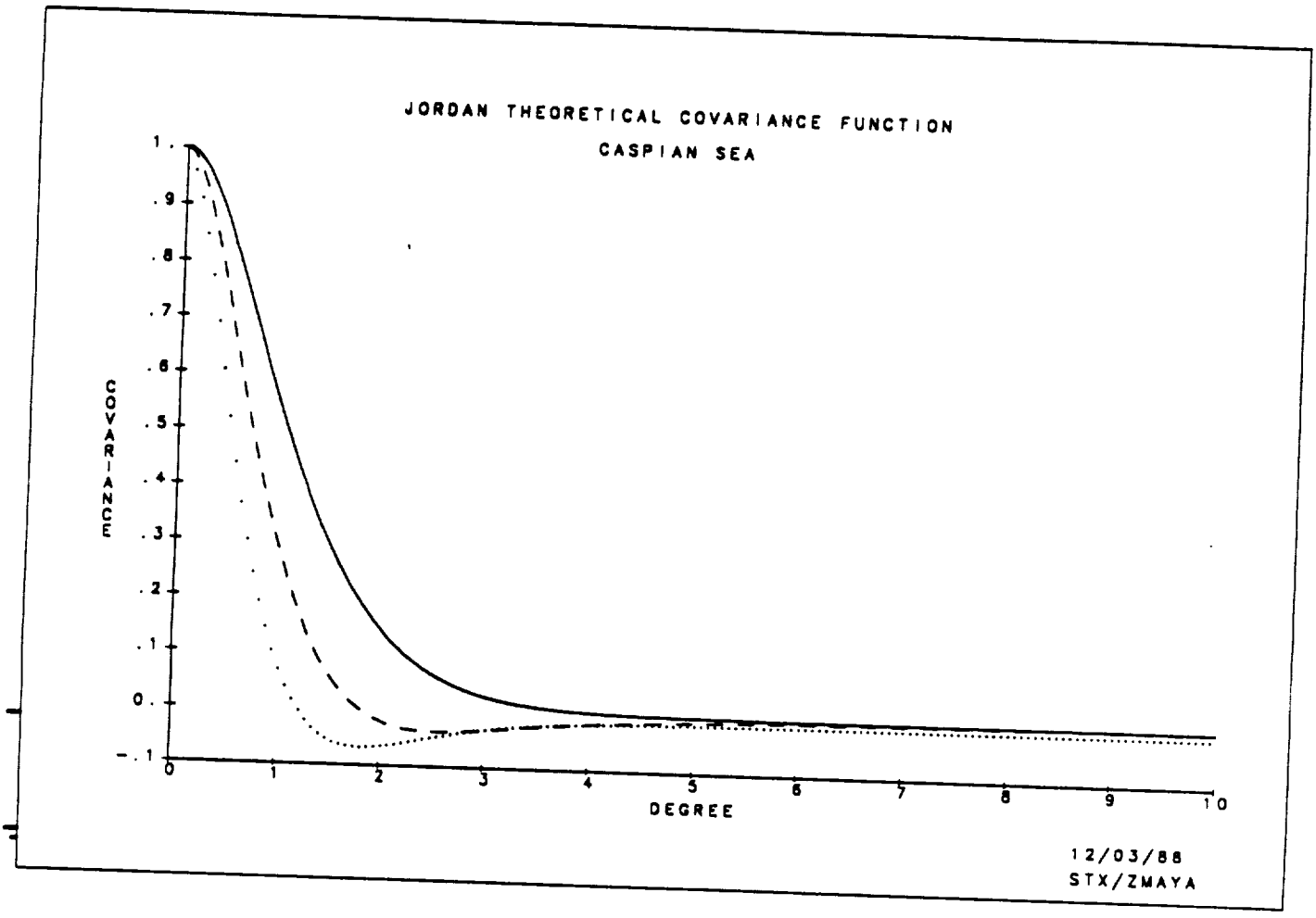

Figure 27. Normalized Jordan's theoretical covariance functions of the Caspian Sea. The normalization coefficients for:

1) undulation-undulation (solid line) is 8.47 m^2,

2) undulation-gravity (dash line) is 43.81 m-mgal, and

3) gravity-gravity (dotted line) is 340.03 $(mgal)^2$.

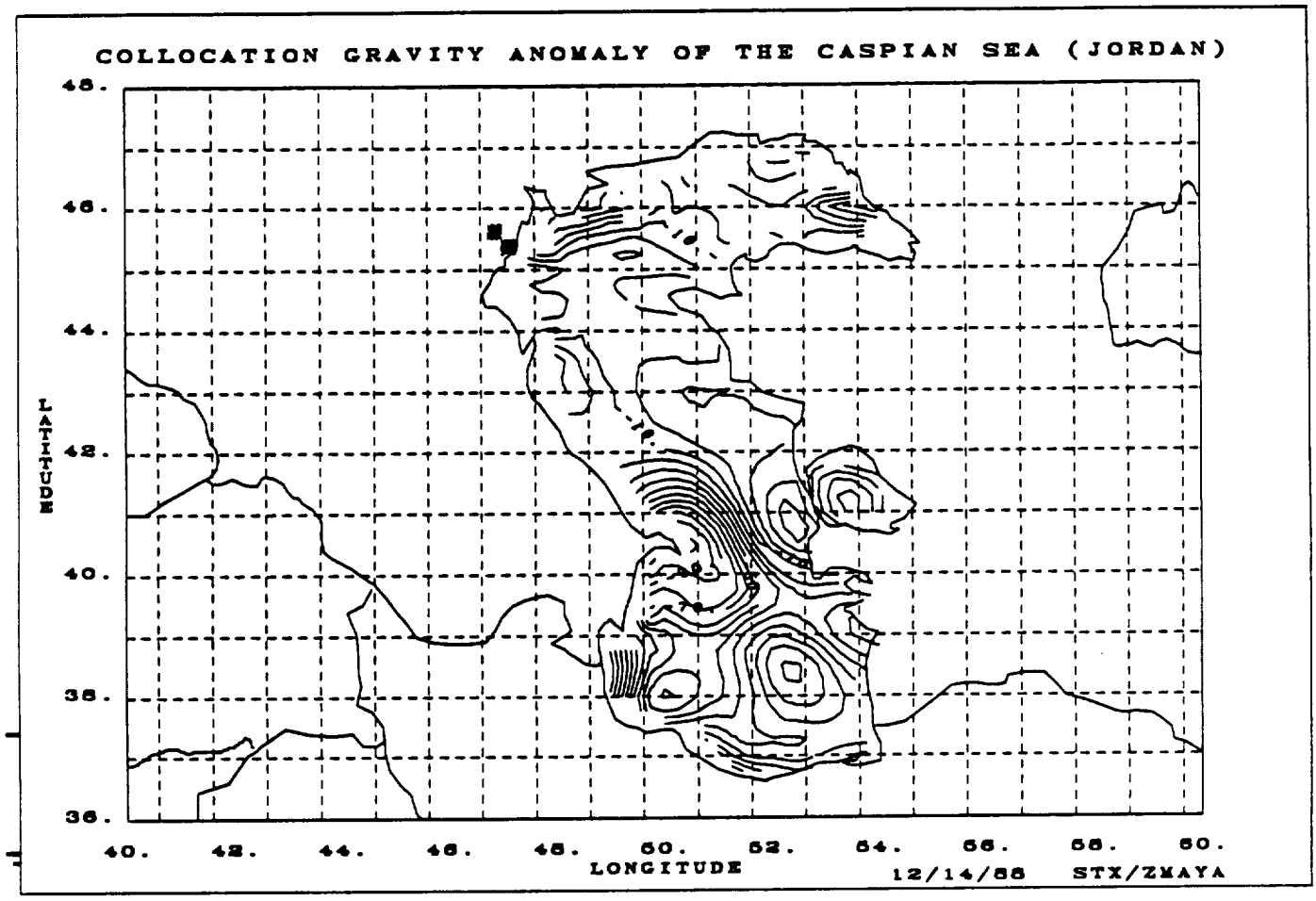

Figure 28. A contour map of estimated gravity anomalies (mgal) of the Caspian Sea based on Jordan's theoretical covariance functions.

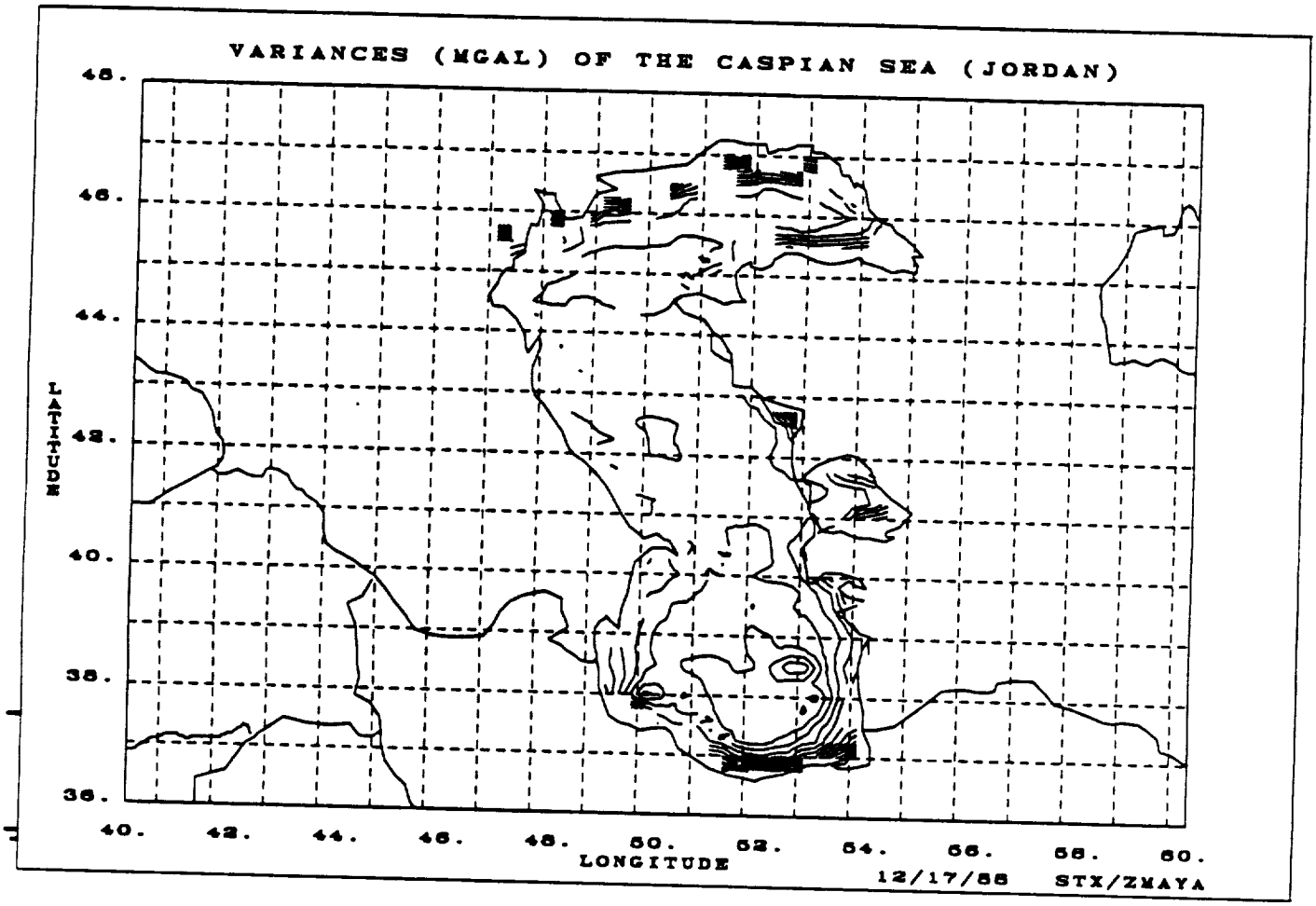

Figure 29. A contour map of the square root of the variances (mgal) of the estimated gravity anomalies of the Caspian Sea based on Jordan's theoretical covariance functions.

larger at 7+ mgal, than that estimated by Rapp's covariance function (Figure 21). These differences are apparently due to differences in un-normalized amplitudes in the respective covariance functions.

The geoid-to-gravity transformation is also performed with local empirical covariance functions. The empirical covariance functions for the Black Sea are shown in Figure 15. Contour maps of gravity anomalies and the square root of the variance for the Black Sea are shown in Figures 30 and 31. The corresponding covariance functions for the Caspian Sea are shown in Figure 16. Corresponding results for the Caspian Sea are shown in Figures 32 and 33. The predicted gravity errors are significantly larger at 7+ and 10+ mgal in the Black and Caspian Seas, respectively, than those predicted by the Rapp or Jordan covariance functions. As before, these increased errors are apparently due to subtle differences in the amplitudes of the covariance functions.

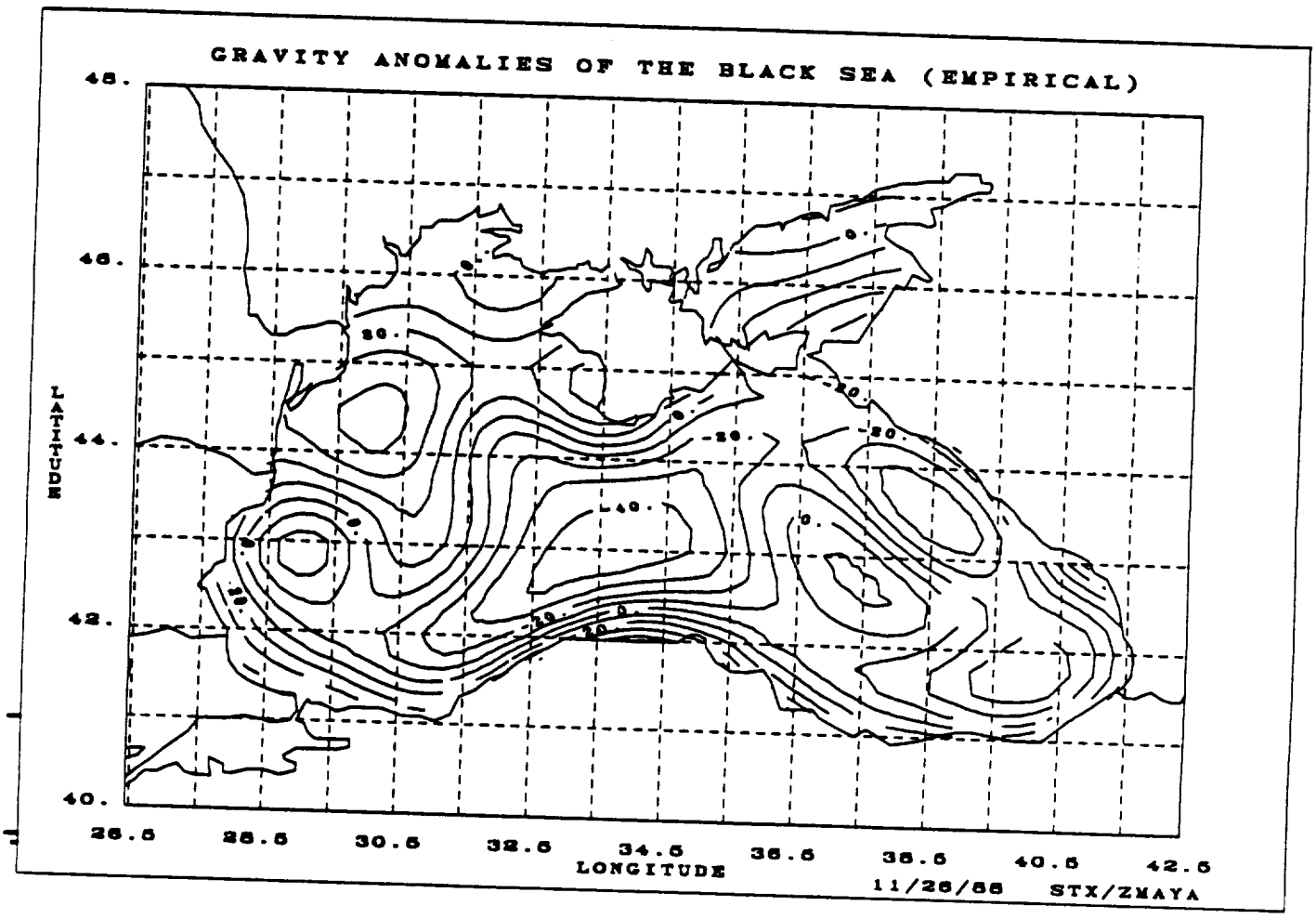

Figure 30. A contour map of estimated gravity anomalies (mgal) of the Black Sea based on local residual empirical covariance functions.

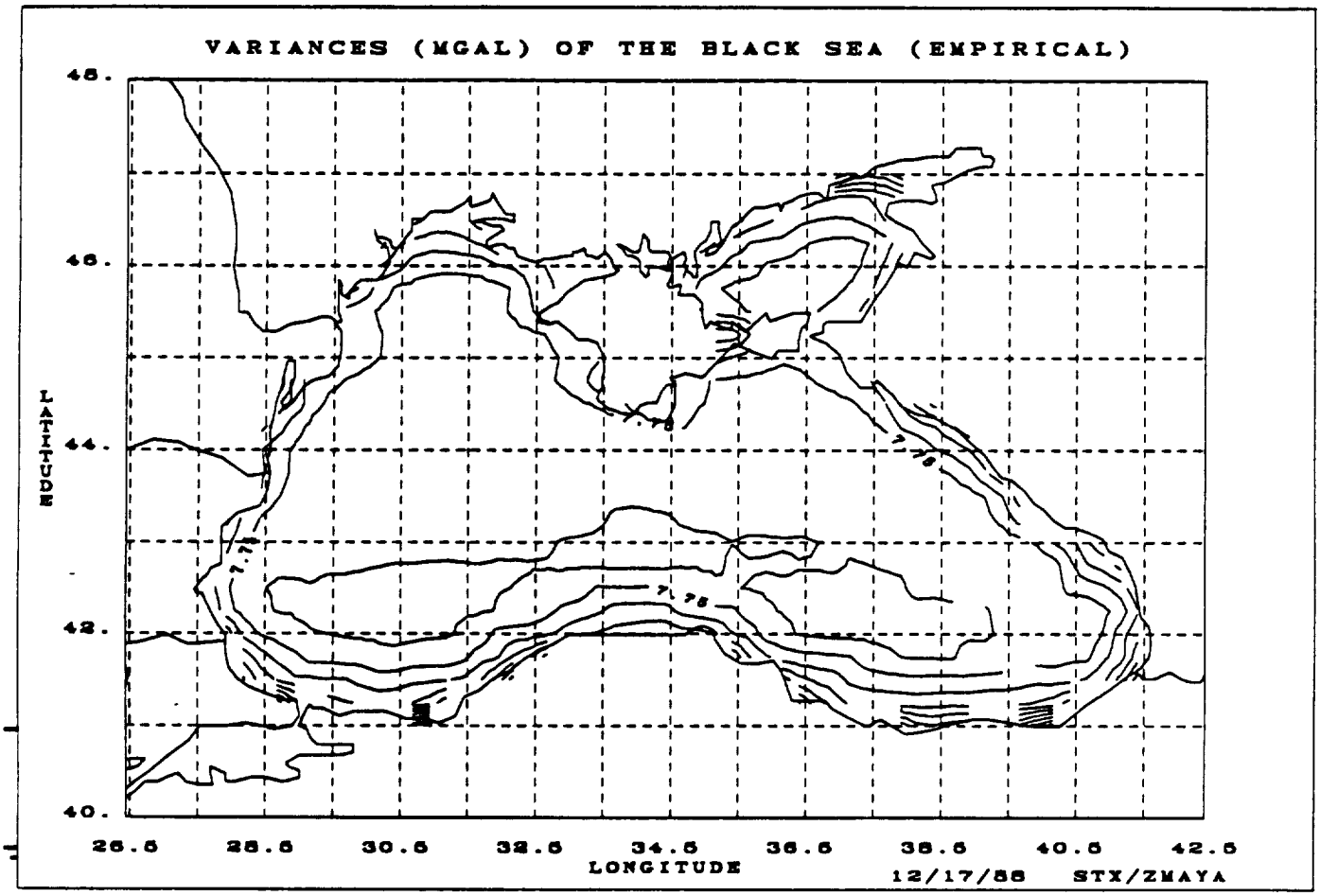

Figure 31. A contour map of the square root of the variances (mgal) of the estimated gravity anomalies of the Black Sea based on local residual empirical covariance functions.

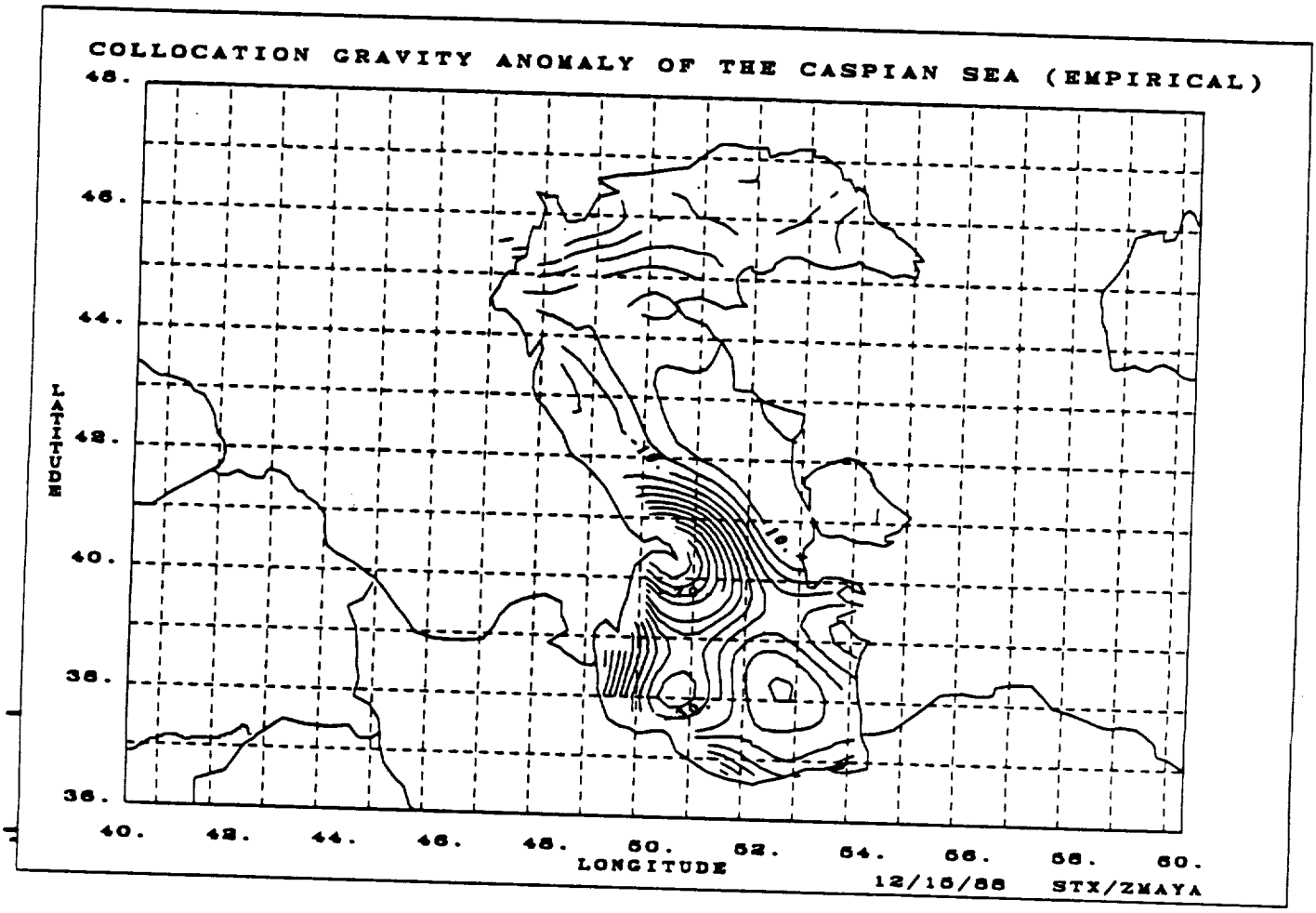

Figure 32. A contour map of estimated gravity anomalies (mgal) of the Caspian Sea based on local residual empirical covariance functions.

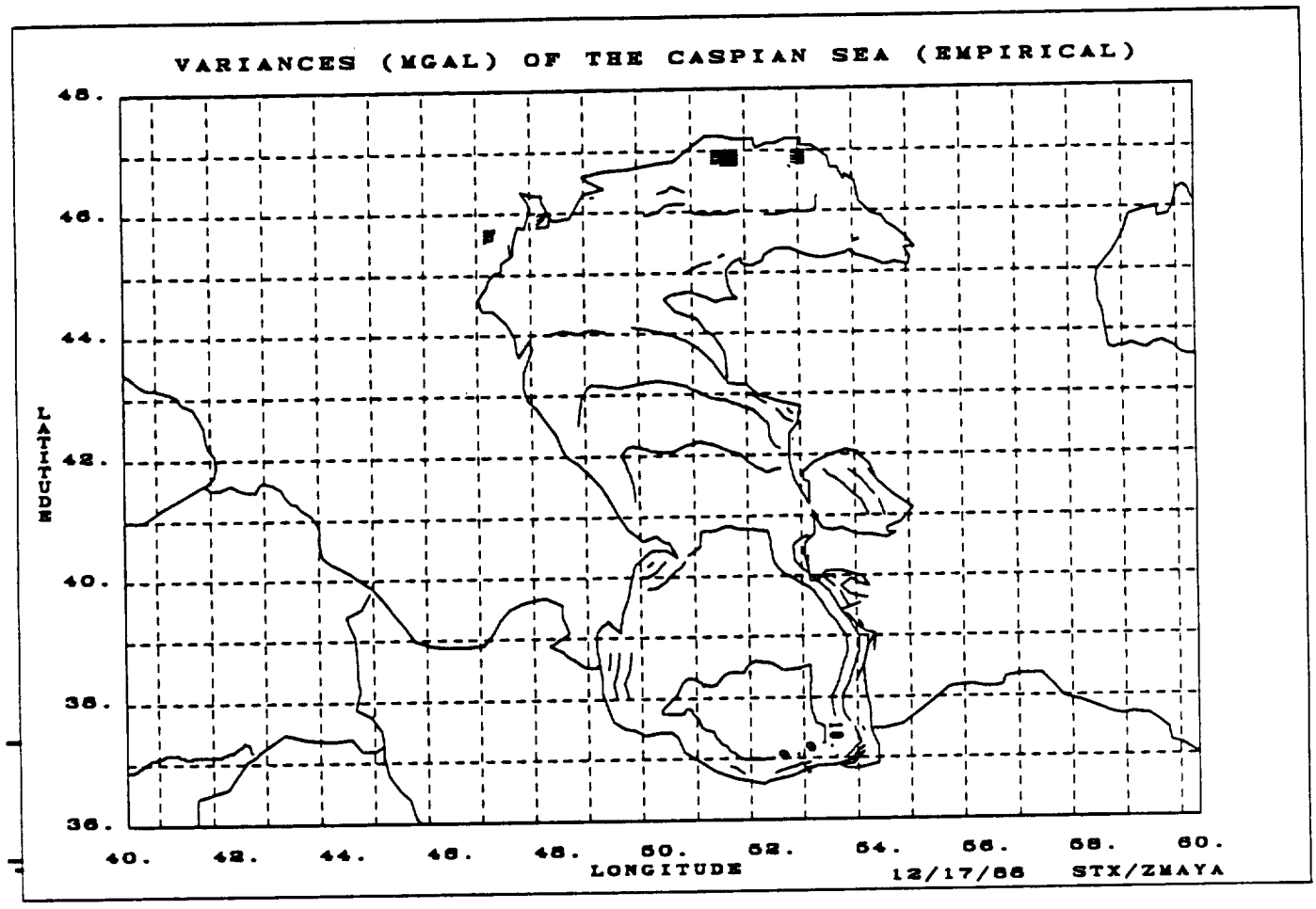

Figure 33. A contour map of the square root of the variances (mgal) of the estimated gravity anomalies of the Caspian Sea based on local residual empirical covariance functions.

V. DISCUSSION

A literature search on collocation techniques and local covariance functions for the geoid and gravity anomalies reveals that local covariance functions vary markedly from one area to another. It should not be a surprise that a single covariance function does not perform equally well for both the Black and Caspian Seas. However, one cannot define a local covariance function for a given area without detailed knowledge of the gravity and geoid heights in the area. This classic "chicken-and-egg" dilemma requires further study. The empirical covariance functions developed for the Black and Caspian Seas (Figures 15 and 16) yield qualitatively good results in that the resulting predicted gravity anomaly map (Figure 30) closely resembles the reference model (Figures 22 and 23) but shows fewer short-wavelength features than the maps predicted using the Jordan or Rapp covariance functions (Figures 25 or 18, and 28 or 20). Comparison of the shapes of these local covariance functions with those of Rapp (Figure 17) or Jordan (Figures 24 and 27) reveal some significant differences. In general, the normalized undulation-gravity covariance function exhibits significantly longer correlation distance (point on the abscissa where the function drops to 0.5) than the undulation-gravity function, which in turn has a longer correlation distance than the gravity-gravity function. This is to be expected due to the integral relationship of geoid undulations to gravity. This relationship holds for the local empirical covariance functions for the Black Sea (Figure 15), but not for the Caspian Sea (Figure 16). The reason for these anomalous properties is not known exactly, but it is suspected that the quality of the reference model in the vicinity of the Caspian Sea is of critical importance. We note that the empirical covariances for the Black Sea behave normally, and there is close agreement between the observed geoid and the model geoid over the Black Sea, in contrast to the striking differences between the observed and model geoids over the Caspian Sea. Over the Black Sea, accurate, short-wavelength geopotential information has been incorporated in Rapp's 180 x 180 geopotential reference model. The altimeter measurements,

represented by the gridded geoid heights, add little new information. This is not the case, however, for the Caspian Sea. It can be concluded that accurate high-frequency information is missing from Rapp's 180 x 180 geopotential model over the Caspian Sea. The quality of the transformation from geoid undulations to gravity anomalies apparently varies depending on the frequency content of the reference geopotential model, calling into question the robustness of the transformation. A consistency test was designed to study the sensitivity of the geoid-to-gravity transformation on the information content (or quality) of the reference model.

A degraded reference model over the Black Sea is obtained by including only long-wavelength (36 x 36) terms of Rapp's 180 x 180 model. Contour maps of the geoid undulations and gravity anomalies of the degraded reference model are shown in Figures 34 and 35, respectively. The geoid-to-gravity transformation is performed based on the degraded reference model and Rapp's 180 x 180 covariance function. The resultant gravity anomalies are shown in Figure 36. It is apparent, comparing with Figure 30, that the quality of the geoid-to-gravity transformation is sensitive to the quality of the reference model. A contour map of the difference between the estimated gravity anomalies using Rapp's 180 x 180 reference model and 36 x 36 reference model is shown in Figure 37. The RMS of the difference is 11.35 mgal, with several broad areas where the difference exceeds 15 mgal.

An iterative transformation to improve the reference model has also been attempted. To evaluate this algorithm in a controlled test, Rapp's 300 x 300 geopotential model is adopted as the true representation of the geoid and gravity over the Black Sea, and the derived geoid surface provides a grid of input data for the geoid-to-gravity transformation and both the 180 x 180 and 36 x 36 models are used as reference surfaces. The iterative method consists of the following steps:

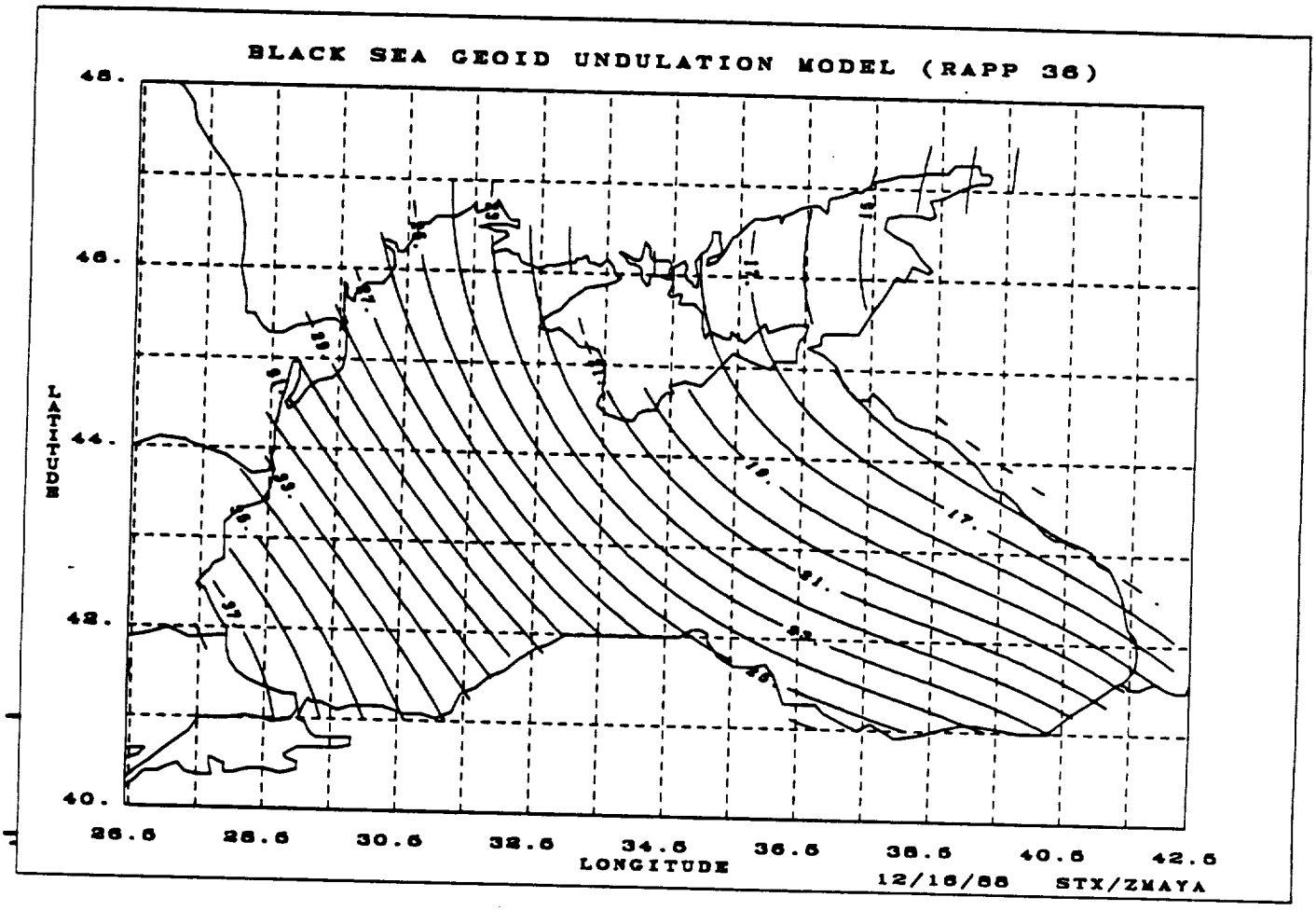

Figure 34. A contour map of Rapp's 36 x 36 reference geoid undulations (m above mean sea level) of the Black Sea.

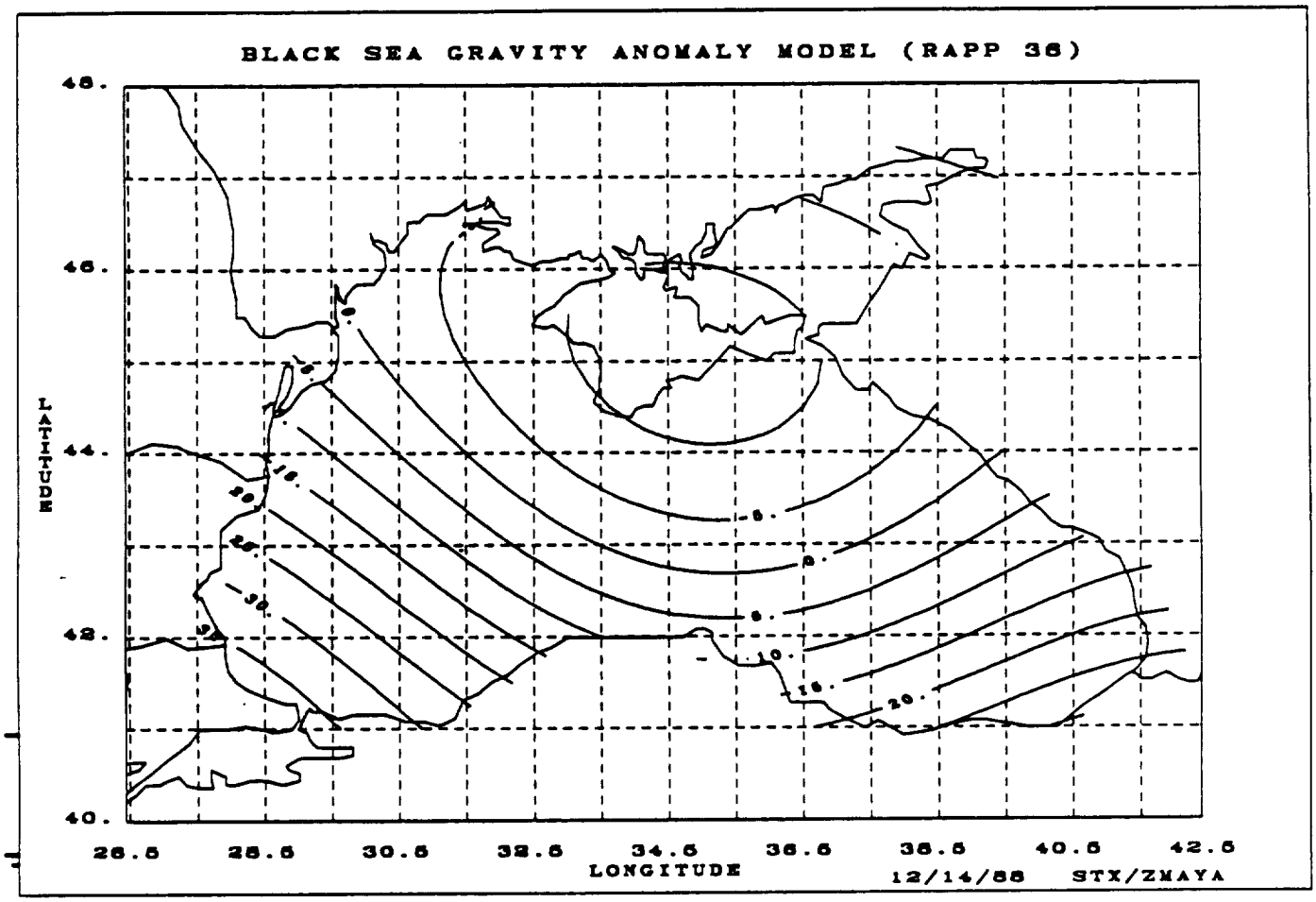

Figure 35. A contour map of Rapp's 36 x 36 reference gravity anomalies (mgal) of the Black Sea.

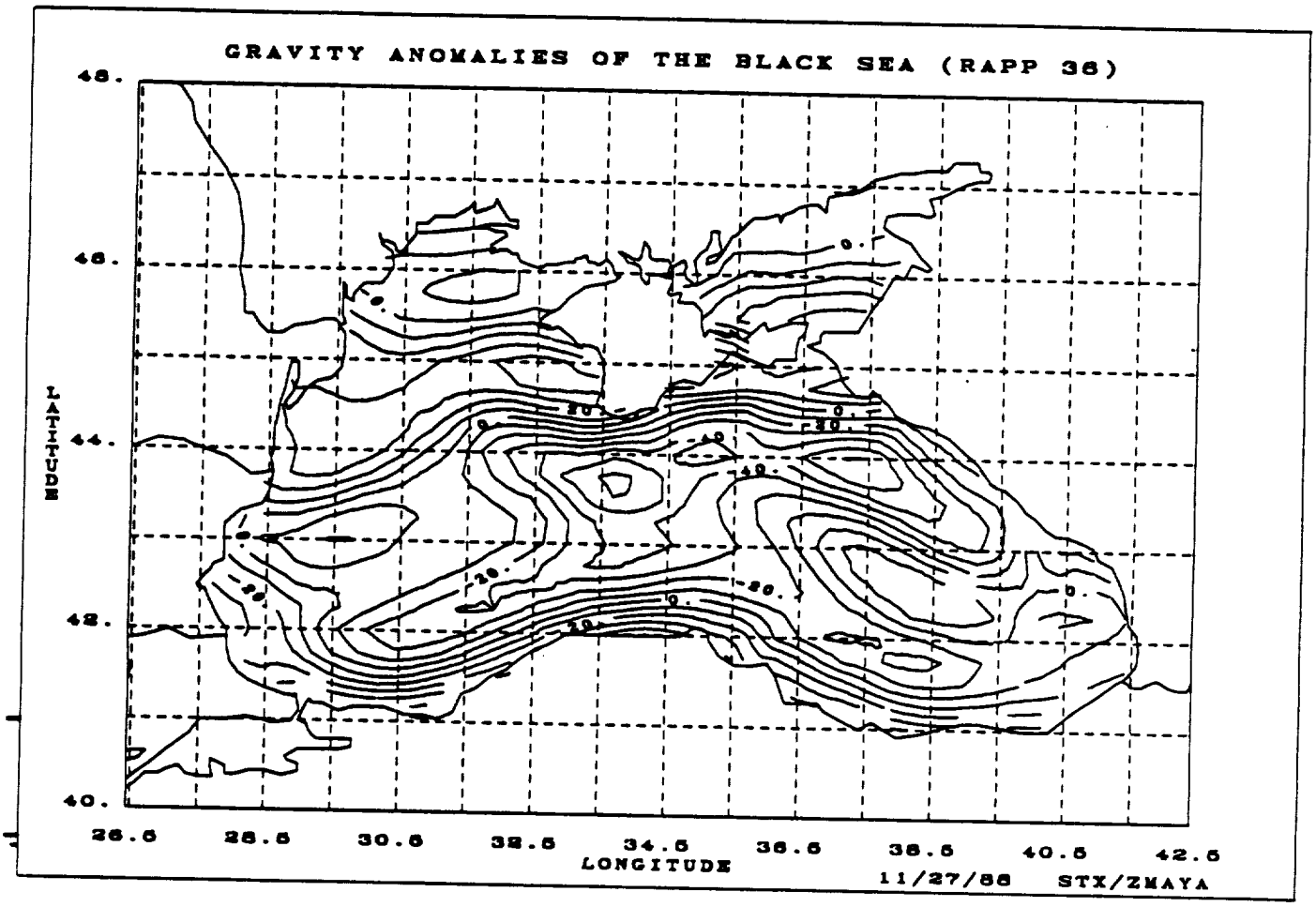

Figure 36. A contour map of estimated gravity anomalies (mgal) of the Black Sea based on Rapp's 36 x 36 reference geopotential model.

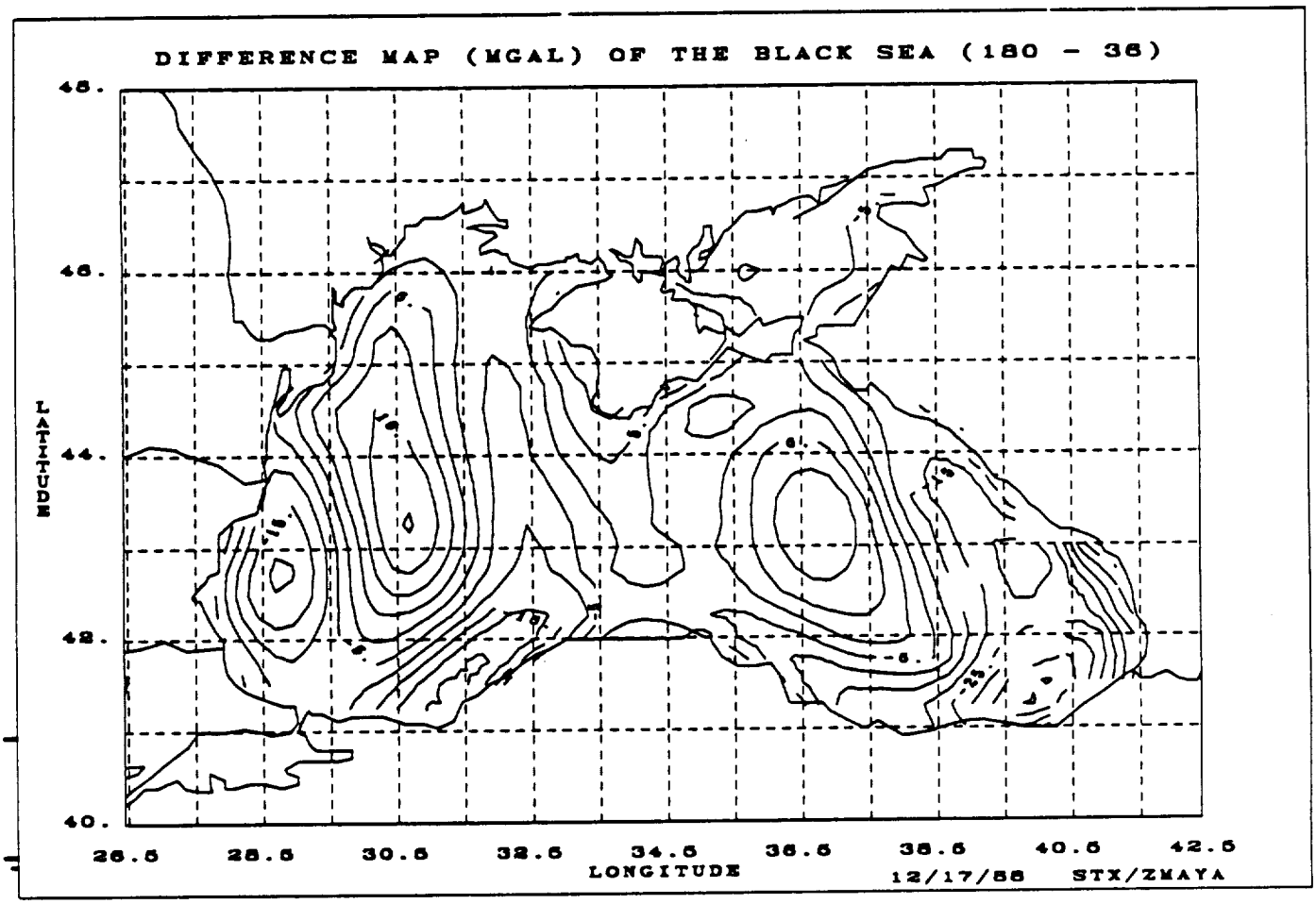

Figure 37. A contour map of the difference (mgal) between estimated gravity anomalies using Rapp's 180 x 180 and 36 x 36 reference models.

a) Use Rapp's covariance function to transform the geoid data to gravity anomalies.

b) Use the same covariance function to transform the gravity anomalies back to geoid heights.

c) Calculate the RMS difference between the transformed result and the reference model for both the geoid and gravity anomalies.

d) Use the transformed gravity anomalies and transformed geoid results to form a new set of local residual empirical covariance functions.

e) Repeat steps a-d using the newly constructed local residual empirical covariance functions for transformation and using the transformed results as the new starting reference model, until the RMS difference satisfies a convergence criterion.

It is observed that using the iterative process for both the 180 x 180 and 36 x 36 reference models, a major correction to the reference models occurs during the first and second iterations. The iterative process converges in less than five iterations for reasonable integration cap radius, such as one degree. The transformed gravity anomalies based on 180 x 180 and 36 x 36 reference models are shown in Figures 38 and 39, respectively. Contour maps of the "true" geoid undulations and gravity anomalies according to Rapp's 300 x 300 model are shown in Figures 40 and 41, respectively. The iterative method does not seem to materially improve the transformation when a poor (36 x 36 compared to 180 x 180) reference surface is used.

The sensitivity of the geoid-to-gravity transformation to different covariance functions and information content of the reference models is quantified by determining the RMS of the difference between the "true" gravity anomalies and the estimated ones, as shown in Table 1. The RMS values represent the error of commission in the geoid-to-gravity transformation. To make the comparison fair, a common *a-priori* stabilizing variance of [25 cm]^2 was added for all three covariance functions when the 180 x 180 reference field was used, and [60 cm]^2 was added whenever the 36 x 36 reference field was used. The iterative algorithm based on empirical covariance functions, compared to the single-pass transformation based on Rapp's and Jordan's covariance functions, generally yields the best recovered gravity anomalies when the information

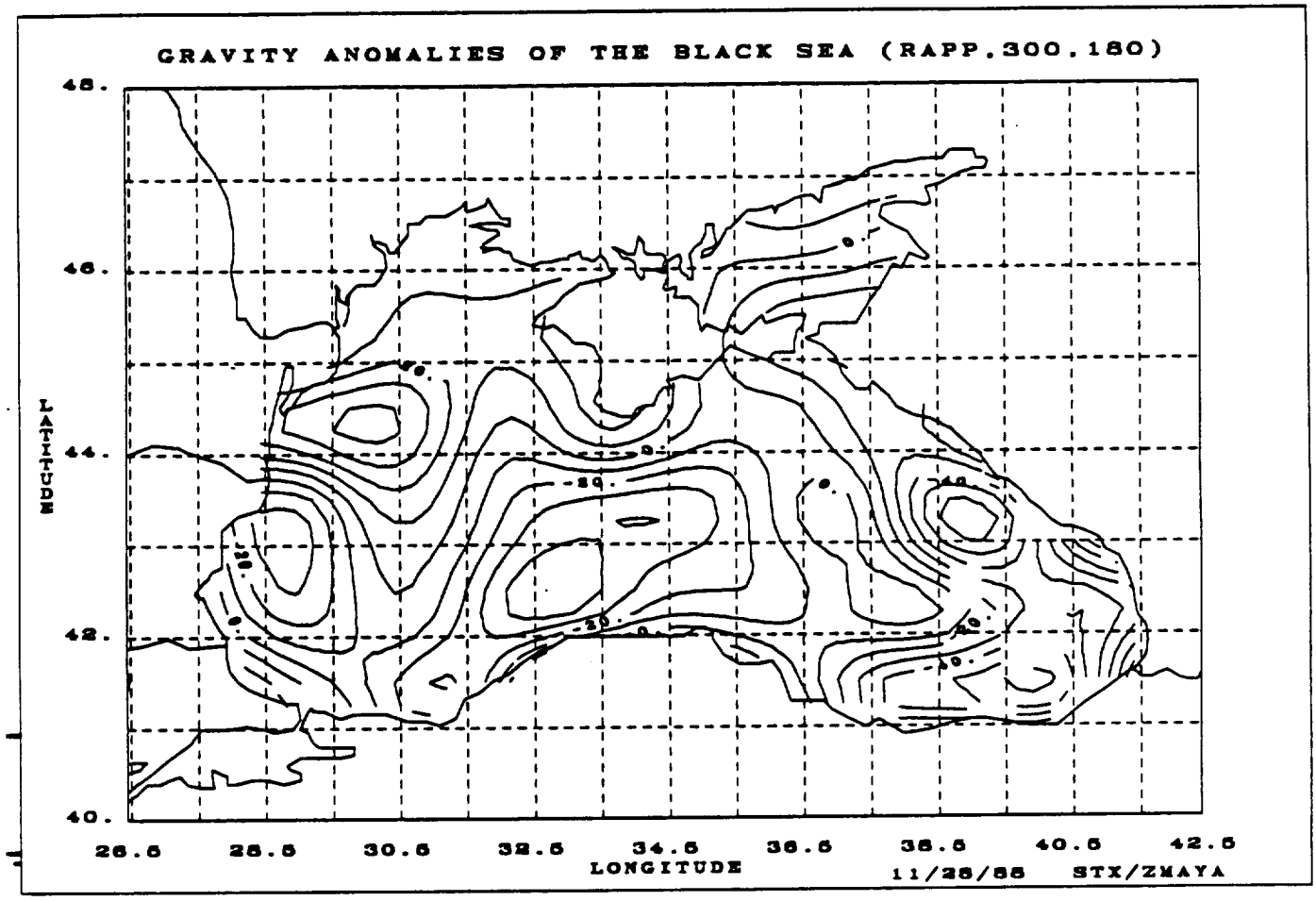

Figure 38. A contour map of the estimated gravity anomalies (mgal) of the Black Sea based on Rapp's 180 x 180 reference geopotential model and the self-consistent iterative approach. Rapp's 300 x 300 model geoid undulations are used as input data. This is a test of the iterative approach.

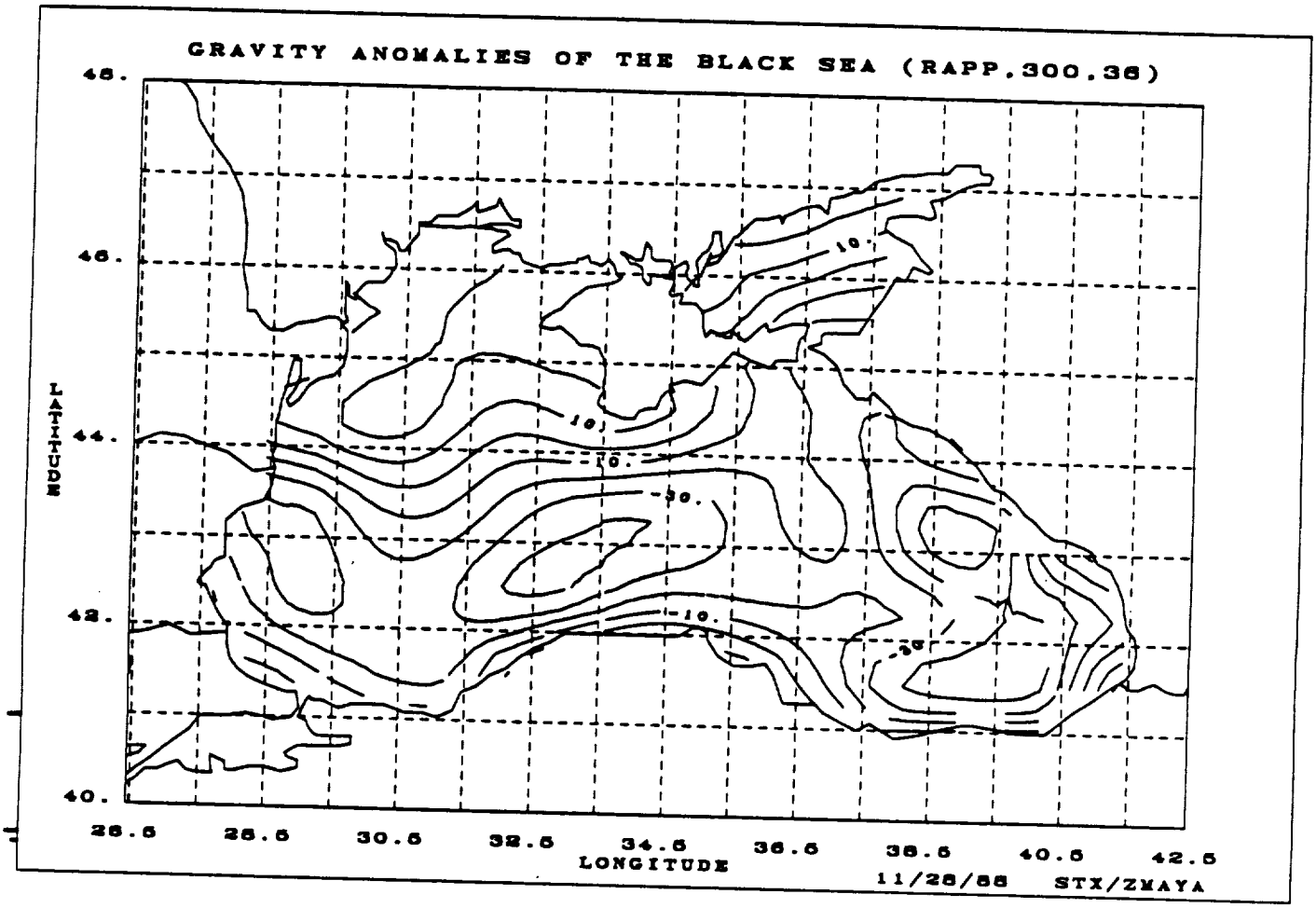

Figure 39. A contour map of the estimated gravity anomalies (mgal) of the Black Sea based on Rapp's 36 x 36 reference geopotential model and the self-consistent iterative approach. Rapp's 300 x 300 model geoid undulations are used as input data. This is a test of the iterative approach.

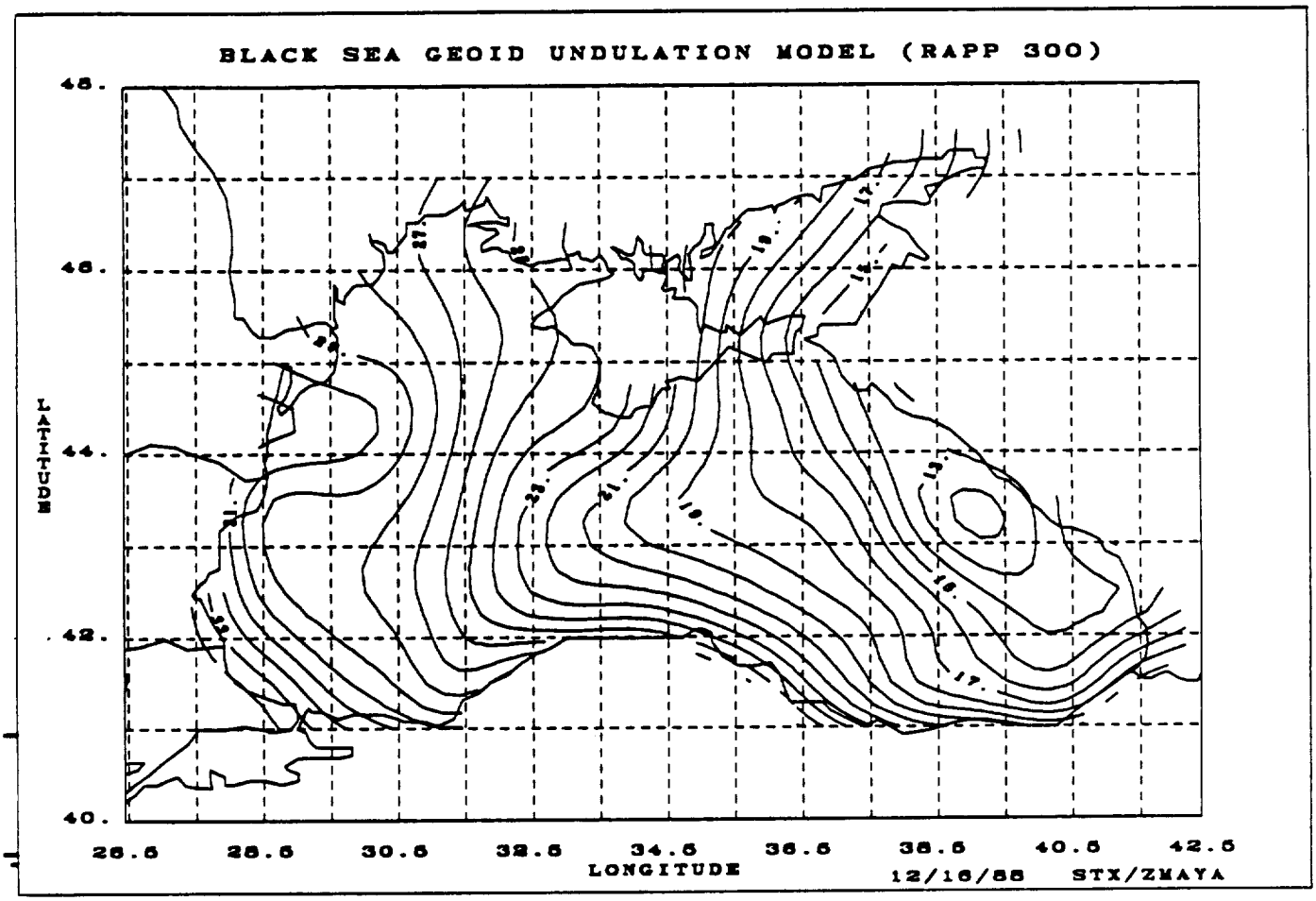

Figure 40. A contour map of Rapp's 300 x 300 reference geoid undulations (m above mean sea level) of the Black Sea.

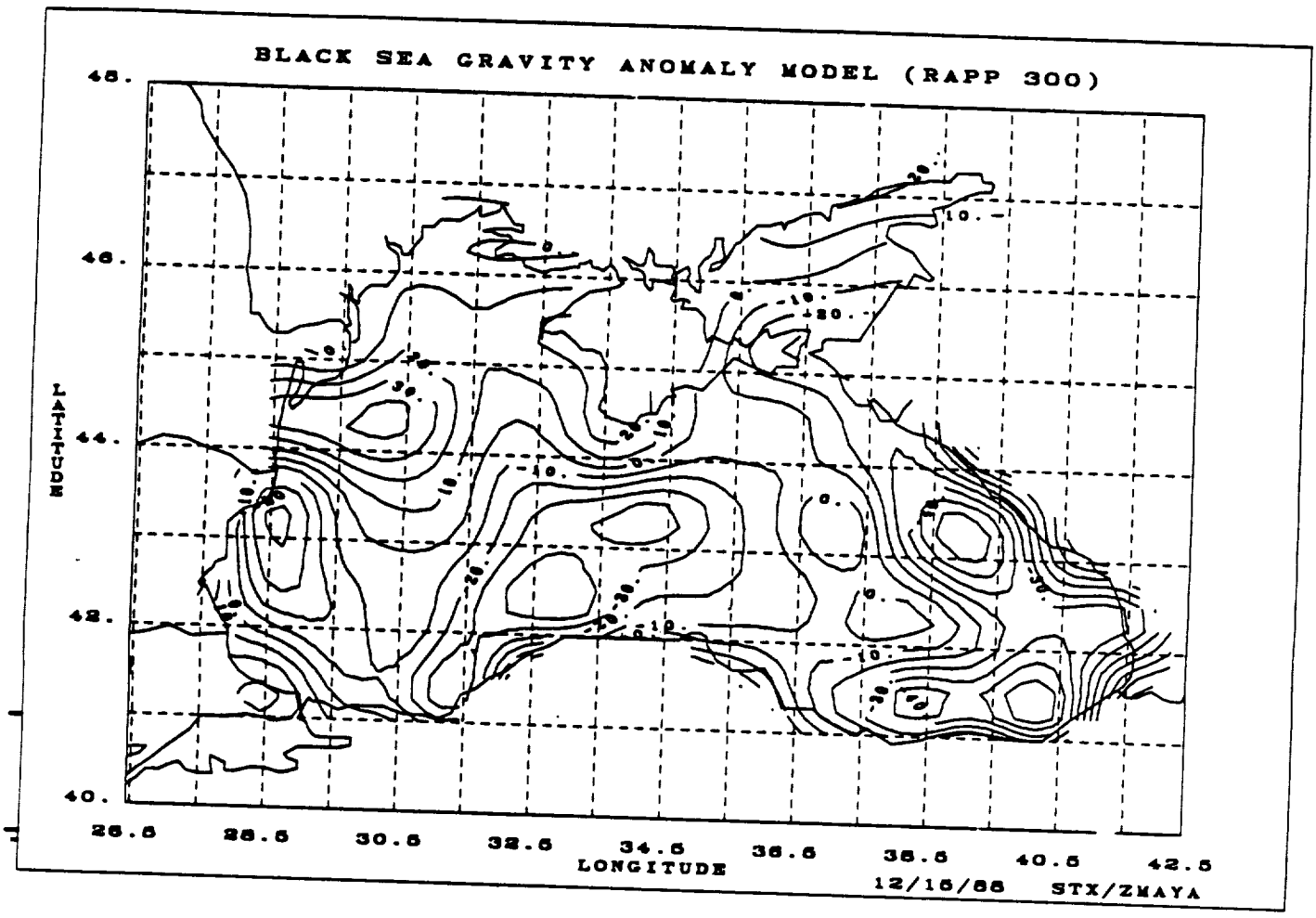

Figure 41. A contour map of Rapp's 300 x 300 reference gravity anomalies (mgal) of the Black Sea.

spectra limit of the reference model is commensurate with the cap size (180 x 180 model and 1° cap size).

transformation covariance functions	180 x 180 reference model (mgal RMS)	36 x 36 reference model (mgal RMS)
Rapp's	4.47	14.39
Jordan's	4.34	11.12
Iterative	3.19	11.79

Table 1 Error of commission in the geoid-to-gravity transformation as a function of different transformation algorithms using 1° cap size for the integration region. Rapp's 180 x 180 and 36 x 36 models are used as reference surfaces.

When the stabilizing *a-priori* error variances are removed or replaced by lower values, while still maintaining solution stability, the RMS error of commission is generally reduced, along with the formal prediction error. For example, in the case of Jordan's covariance function, when the *a-priori* variance is reduced to $(10\ cm)^2$, the corresponding values in Table 1 become 2.97 mgal and 6.96 mgal respectively for 180 x 180 and 36 x 36 reference models. In fact, these levels of stabilizing noise seem to be optimal for both the Jordan and Rapp covariance functions, because lower and higher values of *a-priori* noise result in larger RMS errors of commission. The error of commission for Rapp's covariance function is universally a few percent higher than that for Jordan's covariance function. On the other hand, $(60\ cm)^2$ is optimal (and necessary) for the empirical local covariance function. Based on these results, we conclude that Jordan's covariance function is best for gravity prediction in the Black Sea region, and that the optimal level of *a-priori* noise is about 10 cm. Furthermore, we conclude

that the error of commission of the least-squares collocation technique for gravity prediction is highly dependent on the quality of the reference model, ranging from 3 to 7 mgal.

It should be appreciated that collocation is a statistical method that relies on the transformation covariance functions to provide the physics of the figure of the Earth and its gravity field. The iterative algorithm is a hybrid of a perturbation on the reference surface and an information shaping / filtering process. The initial shaping filter, the covariance function, should conform with the information content of the initial reference surface. That is, for a reference model whose short wavelength cutoff is at 1°, the covariance function should represent information of wavelengths shorter than 1° and the integration cap size should have a commensurate size. It is speculated that when the 36 x 36 model is used as a reference surface, long wavelength correction to the updated reference surface is limited to wavelengths less than 1° because of the chosen integration cap size of 1°. Wavelength components longer than 1° must be corrected in order to improve the 36 x 36 reference model. The integration cap size, therefore, should be relatively large if a long wavelength reference model is to be used. A large integration cap size, unfortunately, will result in forbiddingly high computing costs unless the data grid for the initial iterative steps is decimated. The cap size can be gradually reduced, as the data density is gradually increased, in subsequent iterations. However, an algorithm developed to maintain constant density of data in each iterative step, performed worse than the conventional algorithm.

NASA
National Aeronautics and Space Administration

Report Documentation Page

1. Report No.	2. Government Accession No.	3. Recipient's Catalog No.
NASA TM-100729		

4. Title and Subtitle	5. Report Date
Analysis of Altimetry Over Inland Seas	April 1989
	6. Performing Organization Code: 621

7. Author(s)	8. Performing Organization Report No.
A.Y. Au, R.D. Brown and J.E. Welker	89B00107
	10. Work Unit No.: RTOP #676

9. Performing Organization Name and Address	11. Contract or Grant No.
ST Systems Corporation (STX) Lanham, Maryland	
	13. Type of Report and Period Covered: Technical Memorandum

12. Sponsoring Agency Name and Address	14. Sponsoring Agency Code
Goddard Space Flight Center National Aeronautics and Space Administration Washington, D.C. 20546-0001	

15. Supplementary Notes (continued from block 7)

A.Y. Au and R.D. Brown: ST Systems Corporation (STX), Lanham, Maryland.
J.E. Welker: Goddard Space Flight Center, Greenbelt, Maryland.

16. Abstract

Satellite-based altimetric data taken by GEOS-3 and SEASAT over the Black Sea and Caspian Sea are analyzed and a least-squares collocation technique is used to predict the geoid undulation on a .25-degree by .25-degree grid and to transform these geoid undulations to free air gravity anomalies. This project entailed processing satellite altimeter data over inland seas for recovery of area mean gravity information. Gravity information in this area of the world is not readily available, so the possibility of obtaining it from the processing of altimeter observations is attractive. Our principal objective was to complete and extend analyses done in a previous study, verify those results, and document the results and techniques. A secondary objective was to improve the algorithms and results, if possible. The approach used involved editing geoid height data to remove overland data; evaluating geoid height differences at crossover points; removing orbit errors from geoid heights using crossover differences; gridding geoid height data at .25-degree by .25-degree intervals; and estimating the gravity anomalies from gridded geoid heights using the collocation technique.

17. Key Words (Suggested by Author(s))	18. Distribution Statement
Black Sea, Caspian Sea, gravity anomalies, satellite altimetry	Unclassified - Unlimited Subject Category 46

19. Security Classif. (of this report)	20. Security Classif. (of this page)	21. No. of pages	22. Price
Unclassified	Unclassified		

NASA FORM 1626 OCT 86

VI. REFERENCES

Au, A. Y., R. D. Brown and J. E. Welker (1989) User's Guide. *Programs for Processing Altimeter Data Over Inland Seas.* **NASA Technical Memorandum - 100730.**

Jordan, S. K. (1972) *Self-constant statistical models for gravity anomaly, vertical deflections, and undulation of the geoid.* **J. Geophys. Res.**, 77, 3660-3670.

Knudsen, P. (1987) *Estimation and modelling of the local empirical covariance function using gravity and satellite altimeter data.* **Bull. Geod.**, 61, 145-160.

Moritz, H. (1978) *Least-squares collocation.* **Rev. Geophys. Space Phys.**, 16, 421-430.

Stanley, H. R. (1979) *The Geos 3 Project.* **J. Geophys. Res.**, 84, 3779-3783.

Rapp, R. H. (1986) *Gravity anomalies and sea surface heights derived from a combined GEO-3/SEASAT altimeter data set.* **J. Geophys. Res.**, 91, 4867-4876.

Townsend, W. F. (1980) *An initial assessment of the performance achieved by the SEASAT radar altimeter.* **IEEE J. Oceanic Eng.**, OE-5, 8-092.

Treitel, S. and E. A. Robinson (1966) *The design of high-resolution digital filters.* **IEEE . Trans. on Geoscience electronics**, GE-4, 25-38.

Wagner, C. A. (1979) *The geoid spectrum from altimetry.* **J. Geophys. Res.**, 84, 3861-3871.

PREPARATION OF THE REPORT DOCUMENTATION PAGE

The last page of a report facing the third cover is the Report Documentation Page, RDP. Information presented on this page is used in announcing and cataloging reports as well as preparing the cover and title page. Thus it is important that the information be correct. Instructions for filling in each block of the form are as follows:

Block 1. Report No. NASA report series number, if preassigned.

Block 2. Government Accession No. Leave blank.

Block 3. Recipient's Catalog No. Reserved for use by each report recipient.

Block 4. Title and Subtitle. Typed in caps and lower case with dash or period separating subtitle from title.

Block 5. Report Date. Approximate month and year the report will be published.

Block 6. Performing Organization Code. Leave blank.

Block 7. Author(s). Provide full names exactly as they are to appear on the title page. If applicable, the word editor should follow a name.

Block 8. Performing Organization Report No. NASA installation report control number and, if desired, the non-NASA performing organization report control number.

Block 9. Performing Organization Name and Address. Provide affiliation (NASA program office, NASA installation, or contractor name) of authors.

Block 10. Work Unit No. Provide Research and Technology Objectives and Plans (RTOP) number.

Block 11. Contract or Grant No. Provide when applicable.

Block 12. Sponsoring Agency Name and Address. National Aeronautics and Space Administration, Washington, D.C. 20546-0001. If contractor report, add NASA installation or HQ program office.

Block 13. Type of Report and Period Covered. NASA formal report series; for Contractor Report also list type (interim, final) and period covered when applicable.

Block 14. Sponsoring Agency Code. Leave blank.

Block 15. Supplementary Notes. Information not included elsewhere: affiliation of authors if additional space is required for block 9, notice of work sponsored by another agency, monitor of contract, information about supplements (film, data tapes, etc.), meeting site and date for presented papers, journal to which an article has been submitted, note of a report made from a thesis, appendix by author other than shown in block 7.

Block 16. Abstract. The abstract should be informative rather than descriptive and should state the objectives of the investigation, the methods employed (e.g., simulation, experiment, or remote sensing), the results obtained, and the conclusions reached.

Block 17. Key Words. Identifying words or phrases to be used in cataloging the report.

Block 18. Distribution Statement. Indicate whether report is available to public or not. If not to be controlled, use "Unclassified-Unlimited." If controlled availability is required, list the category approved on the Document Availability Authorization Form (see NHB 2200.2, Form FF427). Also specify subject category (see "Table of Contents" in a current issue of STAR), in which report is to be distributed.

Block 19. Security Classification (of this report). Self-explanatory.

Block 20. Security Classification (of this page). Self-explanatory.

Block 21. No. of Pages. Count front matter pages beginning with iii, text pages including internal blank pages, and the RDP, but not the title page or the back of the title page.

Block 22. Price Code. If block 18 shows "Unclassified-Unlimited," provide the NTIS price code (see "NTIS Price Schedules" in a current issue of STAR) and at the bottom of the form add either "For sale by the National Technical Information Service, Springfield, VA 22161-2171" or "For sale by the Superintendent of Documents, U.S. Government Printing Office, Washington, DC 20402-0001," whichever is appropriate.

National Aeronautics and
Space Administration

Washington, D.C.
20546

Official Business
Penalty for Private Use, $300

Postage and Fees Paid
National Aeronautics and
Space Administration
NASA-451

NASA

POSTMASTER: If Undeliverable (Section 158 Postal Manual) Do Not Return